A Corticostriatal Path Targeting Striosomes Controls Decision-Making under Conflict

Graphical Abstract

Highlights

- A specific fronto-striatal decision circuit is activated by cost-benefit conflict

- It primarily targets striatal striosomes, linked to limbic functions of striatum

- Its optogenetic control selectively alters decisions under cost-benefit conflict

- Its corticostriatal control is exerted through a striatal inhibitory microcircuit

Authors

Alexander Friedman, Daigo Homma, ..., Michael H. Riad, Ann M. Graybiel

Correspondence

graybiel@mit.edu

In Brief

Optogenetic manipulation and electrophysiology of a circuit connecting the prefrontal cortex to striosomes—compartmentalized structures of the striatum—reveals that it has a selective role in influencing decision-making for choices with cost-benefit tradeoffs.

CellPress

Article

Cell

A Corticostriatal Path Targeting Striosomes Controls Decision-Making under Conflict

Alexander Friedman,[1] Daigo Homma,[1] Leif G. Gibb,[1] Ken-ichi Amemori,[1] Samuel J. Rubin,[1] Adam S. Hood[1] Michael H. Riad,[1] and Ann M. Graybiel[1,*]

[1]McGovern Institute for Brain Research and Department of Brain and Cognitive Sciences, Massachusetts Institute of Technology, Cambridge, MA 02139, USA
*Correspondence: graybiel@mit.edu
http://dx.doi.org/10.1016/j.cell.2015.04.049

SUMMARY

A striking neurochemical form of compartmentalization has been found in the striatum of humans and other species, dividing it into striosomes and matrix. The function of this organization has been unclear, but the anatomical connections of striosomes indicate their relation to emotion-related brain regions, including the medial prefrontal cortex. We capitalized on this fact by combining pathway-specific optogenetics and electrophysiology in behaving rats to search for selective functions of striosomes. We demonstrate that a medial prefronto-striosomal circuit is selectively active in and causally necessary for cost-benefit decision-making under approach-avoidance conflict conditions known to evoke anxiety in humans. We show that this circuit has unique dynamic properties likely reflecting striatal interneuron function. These findings demonstrate that cognitive and emotion-related functions are, like sensory-motor processing, subject to encoding within compartmentally organized representations in the forebrain and suggest that striosome-targeting corticostriatal circuits can underlie neural processing of decisions fundamental for survival.

INTRODUCTION

Across the animal kingdom, neural mechanisms have evolved to allow decision-making based on rewarding and aversive features of the environment (Glimcher and Fehr, 2014). This fundamental capacity, critical to normal human life, is disabled in a range of neuropsychiatric and neurologic disorders (Gleichgerrcht et al., 2010). As yet, the mechanisms underlying the relation between decision-making and emotion-related circuit function remain largely unknown (Aupperle and Paulus, 2010). Pioneering work, however, has shown that behavioral reactions to value-based decision-making, based on the perceived potential costs and benefits of taking a given action, are differentially represented in regions of the medial prefrontal cortex (Rangel and Hare, 2010; Rudebeck et al., 2006; Rushworth et al., 2011; Walton et al., 2002). These cortical regions

are interlinked with each other and with other downstream parts of the limbic system (Salamone, 1994; Stopper et al., 2014; Watabe-Uchida et al., 2012). They are also linked to the striatum, part of the basal ganglia (Amemori and Graybiel, 2012; Donoghue and Herkenham, 1986; Eblen and Graybiel, 1995). These networks have been identified in human brain imaging studies as regions of co-activation in relation to emotional task performance (Aupperle et al., 2015; Etkin et al., 2006; Gleichgerrcht et al., 2010). In rodents, potential homologs of these regions of the prefrontal and orbitofrontal cortex have been identified (Milad et al., 2007) and have been particularly intensively studied to identify sub-circuit functions of these networks (Rangel and Hare, 2010; Rudebeck et al., 2006; Walton et al., 2002).

Much anatomical work supports the view that such value-related networks include corticostriatal circuits (Donoghue and Herkenham, 1986; Eblen and Graybiel, 1995; Gerfen, 1984). A striking feature of a subset of these prefronto-striatal and orbitofronto-striatal circuits is that they preferentially target a distinctive set of distributed striatal microzones known as striosomes (Graybiel and Ragsdale, 1978). These regions are distinguishable from the much larger matrix tissue of the striatum by their differential expression of most of the neurotransmitter-related molecules expressed in the striatum (Crittenden and Graybiel, 2011; Graybiel, 1990) and the birth-dates of their neurons (Newman et al., 2015), as well as by their differential inputs and direct and indirect output to parts of the dopamine-containing midbrain (Fujiyama et al., 2011; Prensa and Parent, 2001; Watabe-Uchida et al., 2012) and the lateral habenula (Rajakumar et al., 1993; Stephenson-Jones et al., 2013), regions strongly implicated in the control and modulation of motivation and reinforcement-driven behavior (Hong and Hikosaka, 2013; Lak et al., 2014; Stopper et al., 2014). By contrast, the large matrix compartment of the striatum is divided into a mosaic of microzones known as matrisomes, and these are linked by their outputs to the classic sensorimotor zones of the basal ganglia (Flaherty and Graybiel, 1993).

The differential functions of striosomes, relative to matrix and its matrisomes, have never been identified, largely for technical reasons. Nor is it known how they and their cortico-striatal pathways are recruited in different modes of decision-making related to mood and motivation, despite the fact that it has been known for years that cortical regions targeting striosomes are parts of value-related networks (Rudebeck et al.,
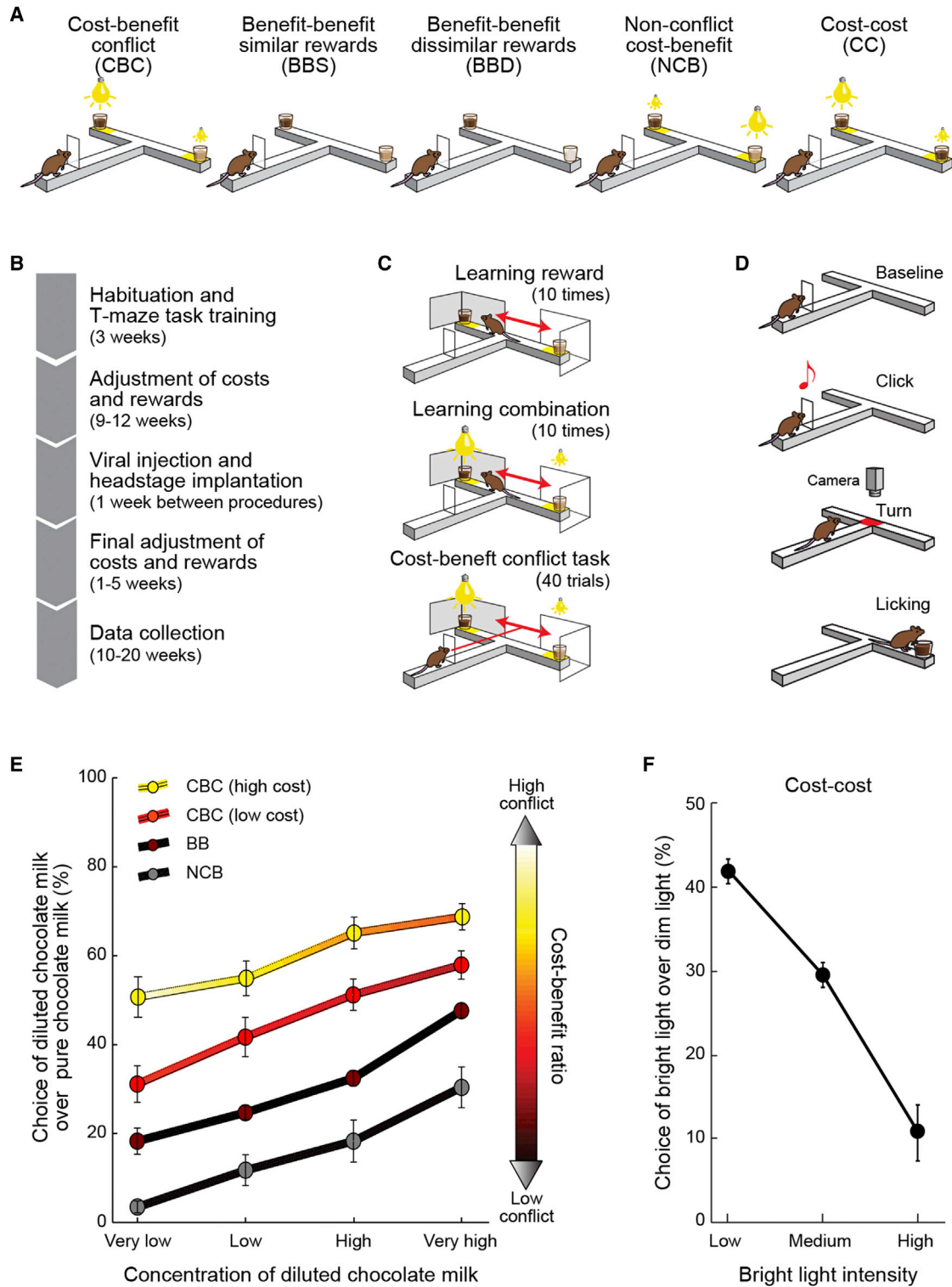
Cell

Figure 1. Decision-Making Tasks

(A) The five decision-making tasks.

(B) Training timeline.

(C) Session of cost-benefit conflict task.

(D) Schematic of maze run.

(legend continued on next page)

2006; Rushworth et al., 2011). The lack of this information presents a major roadblock to the development of neural circuit-based therapies for disorders impacting decisions based on value.

We therefore designed a battery of decision-making tests involving varying combinations of cost and benefit, and then, in rats performing the different tasks, applied an optogenetic approach in order to assess the differential contributions to decision-making of striosome-targeting and matrix-targeting prefrontal corticostriatal pathways. We based our strategy on the finding (Amemori and Graybiel, 2012) that, in monkeys, decisions based on conflicting combinations of cost and benefit in approach-avoidance tasks selectively activate a subset of neurons in a medial prefrontal region that could correspond to a zone targeting the striosome compartment of the striatum, as indicated by earlier anatomical work (Eblen and Graybiel, 1995). These results in the non-human primate suggested that in-depth analysis of striosome-targeting and matrix-targeting circuits with multiple methods feasible in rodent experiments might uncover causally important decision-making control systems hidden from previous analyses.

To do these experiments, we focused on two corticostriatal projections from adjacent prefrontal cortical regions implicated in decision-making (Dwyer et al., 2010; Rudebeck et al., 2006; Seamans et al., 1995; St Onge and Floresco, 2010) and known to have distinct bilateral striatal projection patterns predominantly targeting either striosomes or matrix (Donoghue and Herkenham, 1986; Gerfen, 1984). One, originating in the prefrontal region called prelimbic cortex in rodents (here called PFC-PL), projects preferentially to striosomes in the associative striatum (Donoghue and Herkenham, 1986; Gerfen, 1984). The second, originating in the prefrontal region called in rodents anterior cingulate cortex (here named PFC-ACC), projects preferentially to the matrix compartment of the associative striatum (Donoghue and Herkenham, 1986). By optogenetically tagging these pathways, and then applying manipulations in combination with behavioral and electrophysiological assays, we tried to differentiate the functions of these pathways, identified both by their cortical origins in different medial prefrontal cortical regions and by their different preferential striatal termination fields in either striosome or matrix compartment.

Our findings suggest that the medial prefrontal pathway targeting striosomes is differentially activated by motivational conflict induced by a pair of options evoking approach-avoidance conflict, and that this circuit, by way of an intrastriatal inhibitory network, can control both the activity of striosomes in such cost-benefit decision-making and the behavior itself. These findings place the cortico-striosomal system as a potentially crucial control mechanism for organisms facing the need to act based on conflicting options in their environment.

RESULTS

Rats Develop Distinct, Highly Repeatable Choice Behaviors under Different Cost-Benefit Context Conditions

We challenged rats to make decisions in five different contexts as they performed T-maze tasks in which they could turn right or left to reach one of the offers presented at the end-arm goals (Figures 1 and S1; Supplemental Experimental Procedures). The tasks presented the animals with different combinations of costs and benefits, with lights of different brightness as costs at the end-arm goal sites and chocolate milk of different dilutions as benefits at these sites (Figure 1A). The animals were over-trained (Figure 1B) and were given forced-choice reminder trials before the main experimental sessions (Figures 1C and 1D; Supplemental Experimental Procedures). To estimate the sensitivity of the rats to benefits without accompanying costs, we introduced two benefit-benefit tasks with the end-arms baited with rewards of similar or dissimilar value (Figure 1A). To examine sensitivity to costs, we introduced a cost-cost task, in which benefits were held constant but were paired with different costs (Figure 1A). Finally, to examine how the rats integrated cost and benefit, we introduced cost-benefit tasks (Figure 1A) that allowed us to assess how choice behaviors were affected by different levels of approach-avoidance conflict (Amemori and Graybiel, 2012; Miller, 1971; Vogel et al., 1971). In the cost-benefit conflict task, high benefits were combined with high costs. Thus the rats were required to receive substantial costs to gain reward, a situation inducing approach-avoidance conflict at each choice. In the non-conflict cost-benefit task, high benefits were paired with low costs, thus letting the rats receive reward without receiving substantial costs. In order to estimate the degree of approach-avoidance conflict for these two tasks, we applied logistic modeling and parameterized the cost-benefit ratio (CBR) (Supplemental Experimental Procedures), which indicated the degree of cost that the rats had to accept in order to receive a unit amount of reward. We used the CBR as an estimate of approach-avoidance conflict, because approach-avoidance conflict could be characterized as the conflict between motivation to avoid cost and motivation to approach benefit, and the CBR corresponds to the ratio of these two opponent motivations. This CBR analysis indicated that the conflict task induced high motivational conflict and that the non-conflict task did not (Figure 1E). Our experiments were thus directed toward the form of cost-benefit decision-making in which regulation of simultaneous approach or avoidance motivations was required.

Optogenetic Inhibition of Cortical Input to Striosomes and to Matrix Has Different Effects on Decision-Making Behavior

We analyzed the contribution of the individual striosome-targeting and matrix-targeting pathways first by optogenetically

(E) Choice functions (mean ± SEM) for nine rats for the four tasks including benefit option. Color indicates degree of motivational conflict estimated by logistic modeling.

(F) Choice function (mean ± SEM) for cost-cost task.
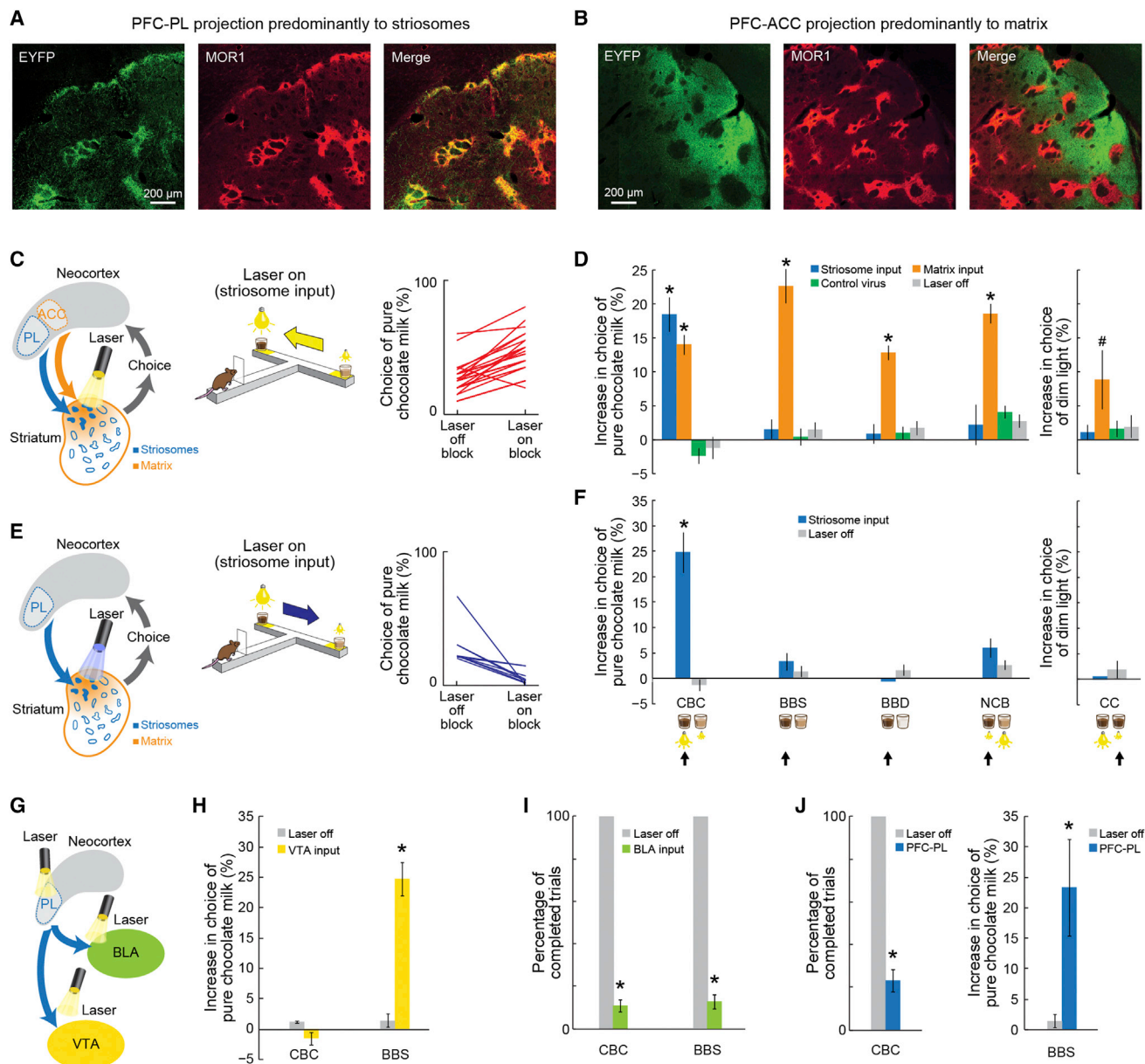
See also Figure S1.

Cell

Figure 2. Optogenetic Manipulation of PFC-PL Cortico-Striosomal Pathway and PFC-ACC Cortico-Matrix Pathway

(A and B) Virally labeled PFC-PL (A) and PFC-ACC (B) corticostriatal projections (green, EYFP-immunostained) preferentially terminating, respectively, in striosome (red, MOR1-immunostained) and matrix compartments.

(C) Intrastriatal inhibition of PFC-PL axons (striosome-predominant input, left) increases choice of high-cost, high-reward option in cost-benefit conflict task (middle). Proportions of choices of such option with and without laser delivery are shown for 25 sessions in ten rats (right).

(D) Behavioral effects of intrastriatal optogenetic inhibition of striosome-predominant PFC-PL inputs (blue) and matrix-predominant PFC-ACC inputs (orange), shown as percentage increase (mean ± SEM) in choice of pure chocolate milk (left) or of dim light (right). #p > 0.07 and *p < 0.001 relative to control groups (green and gray, two-tailed t test).

(E) Intrastriatal stimulation of PFC-PL axons decreases choice of high-cost options in cost-benefit conflict task. Data for nine sessions in three rats.

(F) Intrastriatal inhibition of contralateral striosome-predominant inputs (mean ± SEM). *p < 0.001, two-tailed t test.

(G) Protocol for optogenetic inhibition applied in the PFC-PL or at PFC-PL terminal zones in ventral tegmental area (VTA) or basolateral amygdala (BLA).

(H–J) Behavioral effects (mean ± SEM) of laser delivered in VTA (H), BLA (I), and PFC-PL (J). *p < 0.001, two-tailed t test.

See also Figure S2.

inhibiting their corticostriatal terminal regions in rats with localized injections of adeno-associated virus (AAV5) carrying halorhodopsin (eNpHR3.0-EYFP) under the calcium/calmod- ulin-dependent protein kinase IIα (CaMKIIα) promoter, or control virus, in the PFC-PL or the PFC-ACC, and with optical fibers placed in the anterior dorsomedial striatum (Figures 2A, 2B, and

S2; Supplemental Experimental Procedures). The cortical inputs to the striatum were differentially selective for striosomes in cases with virus-labeled PFC-PL fibers, in accordance with prior findings, and differentially selective for matrix in PFC-ACC cases. However, also in accordance with prior work, the non-preferred compartment always exhibited some labeling, varying case by case (Eblen and Graybiel, 1995; Flaherty and Graybiel, 1991; Gerfen, 1984; Parthasarathy et al., 1992) (Figures S2A and S2B).

Rats with the PFC-PL and PFC-ACC viral injections successfully performed all five decision-making tasks during the optogenetic experiments. In laser-on sessions, a 3-s pulse of yellow light (590 nm, 2 mW) was delivered to the intrastriatal terminal fields from the time of the click indicating trial start to goal-reaching at trial end (Figure 2C). We compared results from blocks of laser-on and baseline trials and from control experiments with viral constructs lacking opsin. Image analysis suggested that within the estimated regions of illumination, the relative density of virally expressed EYFP label was ∼5.2 times higher in striosomes than in the matrix compartment in the PFC-PL cases and ∼2.6 times higher in the matrix than in striosomes in the PFC-ACC cases (Figures S2C–S2E; Supplemental Experimental Procedures). We explicitly chose a block design due to our finding (Figure S1G) that choices from trial to trial within a block were not independent. Moreover, the optogenetic results were not cumulative (Supplemental Experimental Procedures).

Optogenetic inhibition of the striosome-targeting and matrix-targeting circuits had strikingly different effects on decision-making behavior (Figures 2C and 2D). Intrastriatal inactivation of the striosome-targeting PFC-PL pathway strongly affected decision-making in the cost-benefit conflict task: the animals ran more toward the high-cost option, an increase of >20% over control levels (n = 10; Figure 2C). Yet the same intrastriatal manipulation in these animals had almost no effect on their performance of any of the other tasks, including the two other tasks with cost components (Figure 2D). The increased choice of the high-cost, high-reward option induced by inhibiting the PFC-PL pathway to striosomes thus appeared specific to the cost-benefit conflict context, in which the animals had to accept substantial cost to gain reward and had to regulate their approach and avoidance behaviors (Figure 2D).

By contrast, inhibition of the predominantly matrix-targeting PFC-ACC pathway significantly affected the animals' choices in all tasks except the cost-cost task: the animals shifted their choices toward the option with higher reward (n = 8; Figure 2D). In the cost-cost task, there was an increase, not statistically significant (p = 0.07), in the animals' choice of the option with lower cost, perhaps reflecting a partial overlap of the neural representations of higher reward and lower cost in this pathway. Thus the predominantly non-striosome-targeting corticostriatal input to the same dorsomedial striatal region did not exhibit context selectivity comparable to that of the predominantly striosome-projecting circuit.

We took advantage of the patterns of bilateral projection of the PFC-PL and PFC-ACC to perform optogenetic inhibition within the striatum contralateral to the side of virus injection, thus avoiding possible optogenetic effects on corticofugal fibers of passage traveling through the ipsilateral striatum (Figure S2H).

These contralateral manipulations (n = 3) gave the same results as those of the main group of bilateral manipulations: for the PFC-PL circuit, inhibition affected behavior selectively in the cost-benefit conflict task (Figure 2F), and for the PFC-ACC circuit, inhibition affected behavior in all tasks (Figure S2G). These results confirmed that the contrasting patterns of behavior induced by the striosome-targeting and matrix-targeting pathways were not due principally to illumination of bundles of internal capsule fibers within the illuminated zones.

In three rats we applied C1V1-mediated intrastriatal excitation, instead of halorhodopsin-mediated intrastriatal inhibition, to the PFC-PL pathway terminals in the dorsomedial striatum (Figures 2E and S2F; Supplemental Experimental Procedures). The results of the excitatory manipulations were diametrically opposed to those of the inhibitory manipulations: now the rats ran more to the side with low cost and low benefit in the cost-benefit conflict task.

Finally, to test whether the control of conflict decision-making by the striosome-targeting PFC-PL circuit was unique to the striatal terminals of the PFC-PL, we tested whether inhibiting PFC-PL terminals in three other regions to which the PFC-PL projects affected performance on the cost-benefit conflict and benefit-benefit tasks (n = 3 per group; Figure 2G): we inhibited PFC-PL terminals in the ventral tegmental area (Figure 2H), in the basolateral amygdala (Figure 2I) and in the PFC-PL itself (Figure 2J). In none of these experiments was the result of the PL-PFC terminal inhibition similar to the effects of PFC-PL terminal inhibition in the striatum (Figure 2D). Thus the effects of optogenetic inhibition of PFC-PL projections to the dorsomedial striatum were not generalized effects, but rather, were target-specific.

Collectively, these results point to the PFC-PL projection preferentially targeting striosomes as unique among PFC-PL circuits tested in selectively affecting decision-making about approaching or avoiding simultaneously presented, and motivationally conflicting, cost and benefit options.

Experimentally Identified PFC-PL Corticostriatal Neurons and PFC-PL-Targeted Striatal Neurons Have Opposite Firing Patterns during Maze Runs in the Cost-Benefit Conflict Task

To uncover mechanisms that could account for this selectivity, we performed chronic tetrode recordings in the PFC-PL and the striatum (Figures 3 and S3D). We developed an antidromic activation method (Figures 3A and 3B; Supplemental Experimental Procedures) to allow recording of spike activity patterns from identified PFC-PL neurons (here called PFC-PLs neurons) that send axonal projections preferentially targeting striosomes in the dorsomedial striatum and whose terminals were subject to the intrastriatal laser-inhibition in behavioral experiments performed just prior to the antidromic stimulation tests. This strategy allowed us to identify the neurons, among all of the PFC-PL units recorded during the standard five tasks (Figures S3A and S3B), that projected to the dorsomedial striatum.

In the cost-benefit conflict task, high spike activity of nearly all (∼93%) of the 54 cortical PFC-PLs neurons identified occurred in the key period during which the animals initiated their runs and turned to execute their right-left decisions (Figures 3C
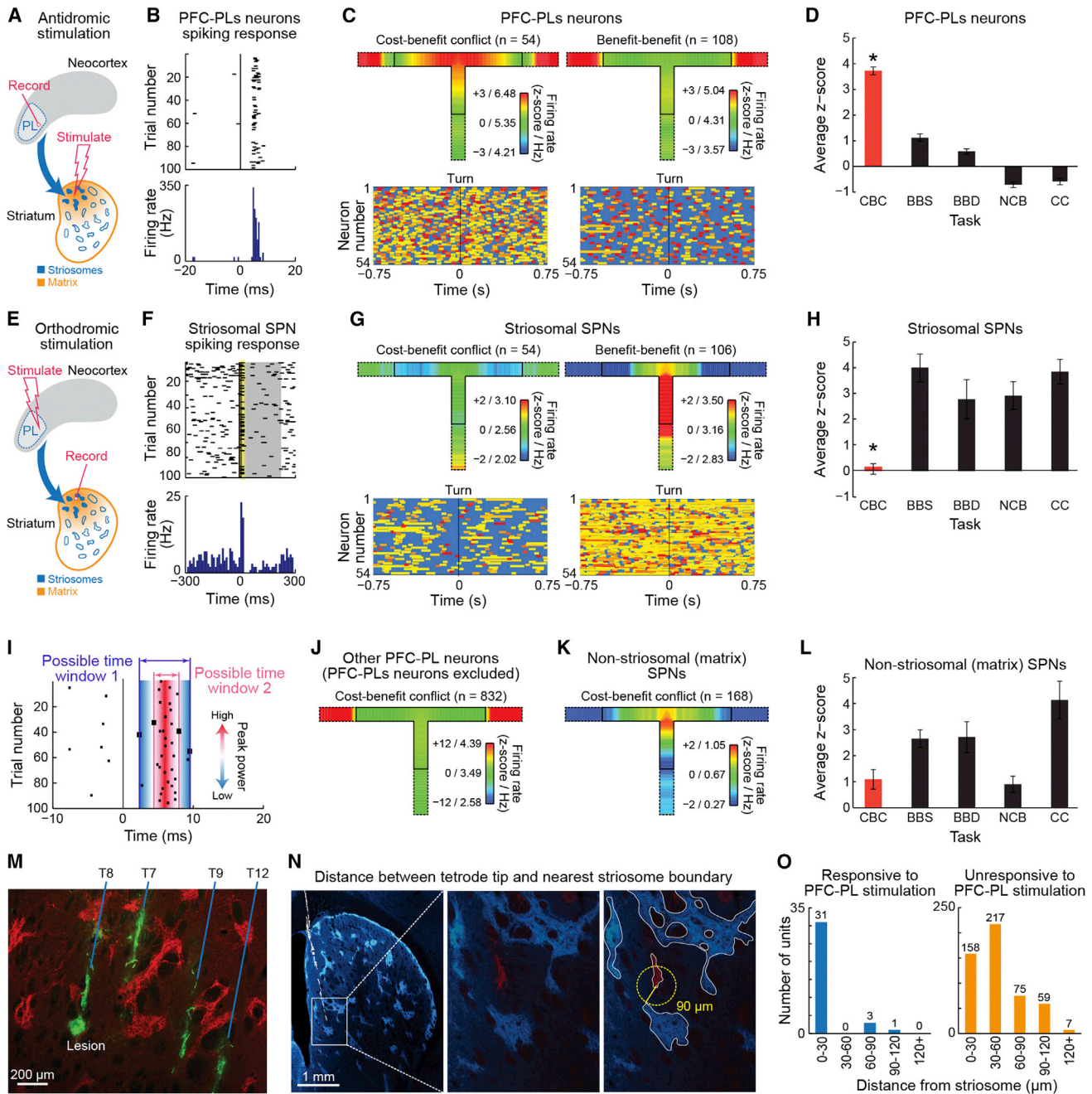
Cell

Figure 3. Contrasting Activity of Putative Cortical PFC-PLs Neurons and Striosomal SPNs during Task Performance

(A) Antidromic stimulation protocol to identify PFC-PLs neurons.

(B) Cortical spikes aligned to striatal microstimulation onset.

(C) Spike activity of PFC-PLs neurons (top) and bursty spike activity heat maps (bottom) in cost-benefit conflict (left) and benefit-benefit (right) tasks. Inner T-maze outline indicates click to first lick (i.e., in-run) time-period; outer outline includes 3 s before and after runs. Activity shown as mean Z scores and firing rates in color scale from blue (low) to red (high). Heat map rectangles show bursts with lengths proportional to burst durations, with min-max normalized intra-burst firing rates from yellow (low) to red (high).

(D) PFC-PLs spike activity (mean ± SEM) during click-to-turn period for all tasks (abbreviated as in Figure 1A). *$p < 0.001$ (two-tailed t test, difference between CBC and each of other tasks).

(E) Orthodromic stimulation protocol for identification of putative striosomal neurons.

(F) Putative striosomal SPN activity aligned to PFC-PL microstimulation. Yellow and gray shading respectively indicates peak and inhibition time windows.

(G) Activity of putative striosomal SPNs (top) and associated burst activity heat maps (bottom).

(H) Average click-to-turn activity of putative striosomal SPNs in the five tasks. *$p < 0.001$ (two-tailed t test; difference between CBC and each of other tasks).

(legend continued on next page)

and S3A). The activity of these neurons peaked in series during this period. In all the other task-versions, PFC-PLs task-related activity was low during this period (Figure 3D), and instead, either peaked at goal-reaching or did not exhibit a significant peak at all (Figure S3A). Thus, the PFC-PLs neuron activity patterns, like optogenetic inhibition of the PFC-PL pathway, pointed to a unique influence of this striosome-targeting pathway on performance of the cost-benefit conflict task.

Identifying the activity of striosomal neurons themselves during task performance would provide a critical test of the selectivity of the effects of PFC-PLs neurons on striosomes. However, chronic in vivo recording from striosomes has never before been achieved. We attempted to do this by capitalizing on the preferential PFC-PL inputs to striosomes demonstrable anatomically (Figures 2A and S2; Supplemental Experimental Procedures). We applied electrical stimulation to the PFC-PL region that we had identified as projecting predominantly to striosomes in the dorsomedial striatum (Figures 3E and 3F), and we simultaneously recorded from large numbers of striatal projection neurons (SPNs) (Figure S3E) in rats with arrays of tetrodes chronically implanted in the dorsomedial striatum (Figure 3M). At the end of each session, we determined for each SPN whether it had short latency responses to the PFC-PL stimulation (Figures 3E, 3F, and 3I), then marked some of these tetrode tip locations with lesions (Figure 3M) and in histologically prepared brain sections mapped these locations relative to immunostained striosomes (Figure 3N). We found a reliable orthodromic response signature of putative striosomal SPNs so identified (Figure 3O; Supplemental Experimental Procedures).

Given that the corticostriatal projection to SPNs is glutamatergic and excitatory, we expected that the activity of these putative striosomal SPNs would match that of the antidromically identified PFL-PLs neurons. We found the opposite. During the in-run period during which the PFC-PLs neurons were highly active (Figure 3C), the striosomal neurons were largely quieted (Figure 3G). Yet ∼98% of striosomal SPNs exhibited high activity during this click-to-turn period in all of the other task-versions, again peaking at different points during this period (Figures 3H and S3F). Thus, the striosome-projecting PFC-PLs neurons and the striosomal SPNs to which they mainly projected had almost perfectly complementary patterns of activity during the maze runs.

To test the selectivity of these patterns, we analyzed the activity of the PFC-PL neuronal population as a whole, excluding the 54 antidromically identified PFC-PLs neurons. In sharp contrast to the PFC-PLs cells, this PFC-PL population fired at goal-reaching in every task (Figures 3J, S3B, and S3C). Thus, the PFC-PLs in-run activity pattern was highly selective. We also analyzed the activity of striatal SPNs excluded from the putative striosomal

SPN population (Figures 3K, 3L, S3G, and S3H). In contrast to the population of putative striosomal SPNs, the striatal neurons identified as non-striosomal SPNs, which should mostly have been matrix neurons, were active in all tasks (Figures 3L and S3G; Supplemental Experimental Procedures), and their activity tended to be selective for choices of higher reward (Figure S3H). These activations were significantly different from baseline activity (two-tailed t test, $p < 0.001$), and their response patterns for the five tasks were significantly different from those of the putative striosomal SPNs (MANOVA and two-way ANOVA, $p < 0.001$).

As shown in Figure S3, baseline activity was not uniform across all tasks, being particularly low in the non-conflict cost-benefit task and the cost-cost task and especially for PFC-PLs neurons. To test the possibility that baseline firing rates might influence our optogenetic results, we compared baseline firing rates during consecutive laser-off and laser-on trial blocks. Despite the large changes in behavior induced by the optogenetic manipulation, baseline rates for both the putative striosomal neurons and the putative matrix neurons were unaffected (Supplemental Experimental Procedures).

Switching of Striosomal Neuron Activity Patterns Can Be Induced by Behavioral Task Switches Alone and by Optogenetic Inhibition of PFC-PLs Inputs Preferentially Targeting Striosomes

If, as these results suggested, the striosomal SPNs were uniquely sensitive to the conflict context, then it should be possible to demonstrate such sensitivity at a single-unit level by recording for prolonged periods extending through consecutive performance of benefit-benefit and cost-benefit conflict sessions. We succeeded in doing this for ten SPNs recorded in two rats (Figure 4A). Strikingly, all of these putative striosomal SPNs, identified by post-performance template tests, switched their firing patterns depending on the task being performed, from being active during the click-to-turn period in the benefit-benefit task to being nearly silent during the same click-to-turn period in the succeeding cost-benefit task (Figures 4B-4E). The switch was nearly immediate (Figure 4C). Such firing switches did not occur when the two blocks were of the same task-type (Figure S4). Thus, the spike-firing patterns of putative striosomal SPNs can be dynamically determined by behavioral context alone.

Next we asked whether the complementarity of firing of the striosomal SPNs and the PFC-PLs neurons reflected an inhibition of the striosomal SPNs by the PFC-PLs neurons. If so, optogenetic inhibition of the PFC-PLs input during the cost-benefit conflict task might increase the run-period activity of striosomal SPNs, thereby abolishing the unique lack of such activity in the

(I) Method to determine time-window of short-latency orthodromic SPN activation (Supplemental Experimental Procedures). Larger squares show spike times demarcating start and end of time window.
(J and K) Average spike activity of non-PFC-PLs population recorded in PFC-PL (J) and putative matrix SPNs (K) during cost-benefit conflict task.
(L) Average click-to-turn activity of putative matrix SPNs.
(M) Four tetrode tracks and tip marked with micro-lesion (CD11, green) relative to striosomes (MOR1, red).
(N) Sample of tip-striosome measurements (Supplemental Experimental Procedures). Tetrode tip in matrix (red, middle and right panels) along tetrode track (white, left panel); distance to nearest striosome (light blue) shown (yellow line).
(O) Distribution of SPNs that respond to PFC-PL stimulation (left) was significantly different from that of unresponsive SPNs (right; $p < 0.001$, chi-square test). See also Figure S3.
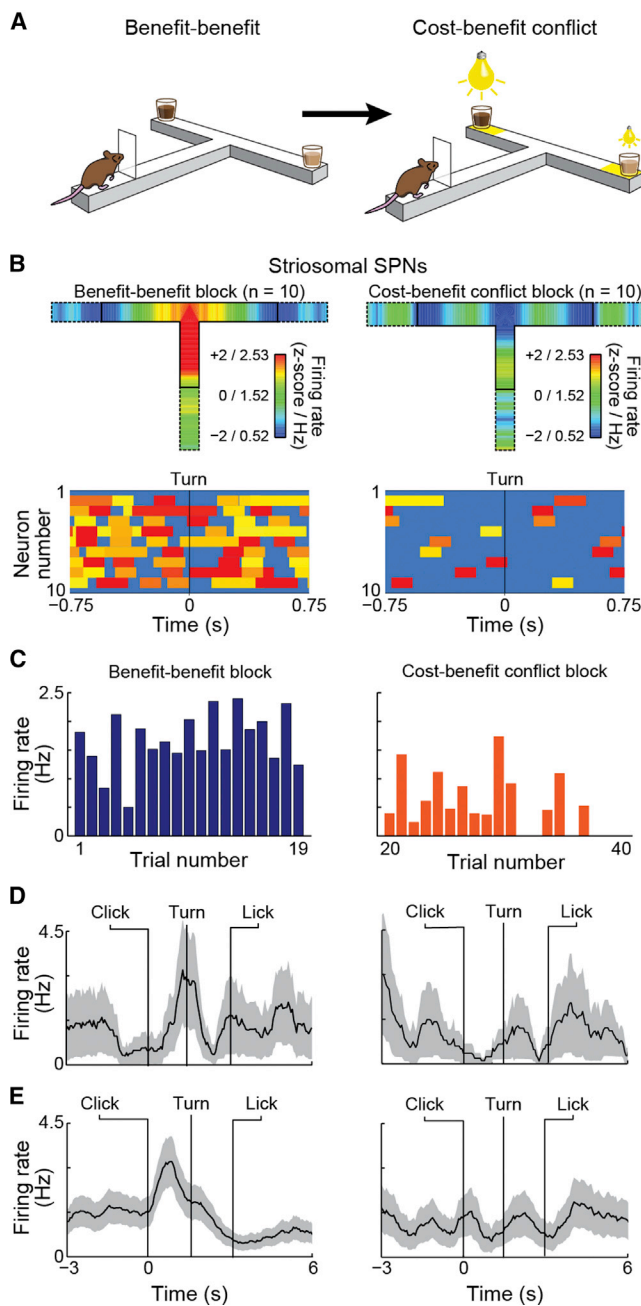
Cell

Figure 4. Activity of Putative Striosomal Neurons Changes with Switch to Cost-Benefit Conflict Task

(A) Timeline for benefit-benefit task (19 trials) followed by cost-benefit conflict task (21 trials). Reminder trials were given in-between.

(B) Average activity of 10 striosomal SPNs held through both blocks (above) and burst activity heat maps (below).

(C) Average in-run firing rates in each trial through the two tasks. p < 0.001, paired t test between blocks.

(D and E) Firing rates (mean ± SEM) of one (D) and ten (E) putative striosomal SPNs recorded across the two tasks. p < 0.001, paired t test between blocks. See also Figure S4.

cost-benefit conflict task (Figure 5A). We observed just such dynamic switching in two rats in which we performed tetrode recordings simultaneously during the optogenetic inhibition: 46 of 49 putative striosomal SPNs responded with increased activity during laser-on trials (Figures 5B–5E). The optogenetic inhibition transformed the striosomal SPN task-related activity into a pattern similar to that normally observed in the other task-versions, with peak activity during the runs (Figure 3G). The optogenetic effect on the firing rate of striosomal SPNs and the choice behavior was nearly immediate (Figures 5C and S5A), but baseline firing rates of these neurons were not affected (Figure S5B). These results demonstrated that the absence of putative striosomal activation in the cost-benefit conflict task could be due to the activation of the PFC-PLs circuit.

High-Firing Striatal Interneurons Exhibit Differentially High Burst-Firing Activity during Cost-Benefit Conflict Task Performance

The spontaneous and optogenetically induced switches in the firing patterns of striosomal SPNs during task performance suggested that these SPNs are under dynamic control by striatal inhibitory microcircuits that themselves are context-sensitive. To test this idea, in the multi-tetrode recordings we searched for and identified putative striatal interneurons (HFNs), known for their high firing rates and thought to exert inhibitory control over striatal SPNs (Berke, 2011; Burguière et al., 2013; Kita and Kitai, 1988; Koós and Tepper, 1999) (Figure S3E). We examined their task-related burst-firing patterns in the five different task-versions (Figures 6A, 6B, and S6F). The putative HFNs, like cortical PFC-PLs neurons, had high firing rates during runs in the cost-benefit conflict task, and in particular, high rates of bursty firing as defined by an in-house algorithm (Figures S6A–S6E; Supplemental Experimental Procedures). The high burst activity of the HFNs occurred principally in the cost-benefit task; in the other task-versions, their intra-burst firing rates were low, relative to baseline intra-burst firing rates (Figures 6A, 6B, and S6F). These sharp, task-dependent differences were not obvious in the overall firing rates. The similarity of the burst activity patterns of the HFNs to the PFC-PLs patterns suggested that the PFC-PLs cells might excite these HFNs, leading to the suppression of the SPN firing that we had observed.

To test this possibility, we searched for pairs of HFNs and SPNs recorded simultaneously on single tetrodes, concentrating on the cost-benefit conflict task. When we aligned the spikes of the SPNs to the peak firing of the HFNs, profound inhibition of the SPNs was apparent (Figures 6C and S6G). Across the population of 23 SPN-HFN pairs, the degree of inhibition of the SPN firing was highly correlated with the burst firing rates (Figures 6D and S6H), but not the tonic firing rates, of the HFNs. We also searched for pairs of HFNs and PFC-PLs neurons recorded simultaneously in the same animal. In these pairs, PFC-PLs activity peaks preceded the HFN peaks (Figure 6E), which occurred in a temporal succession from ~2 s before the start click to ~3 s after the click, and the striosomal SPNs were then inhibited. Experiments with electrical microstimulation of PFC-PL suggested that HFN activation led SPN activation by ~3 ms (Figure 6F), and combining such microstimulation with intrastriatal optogenetic inhibition (Figure 6G) led to an increase in firing of the SPNs,
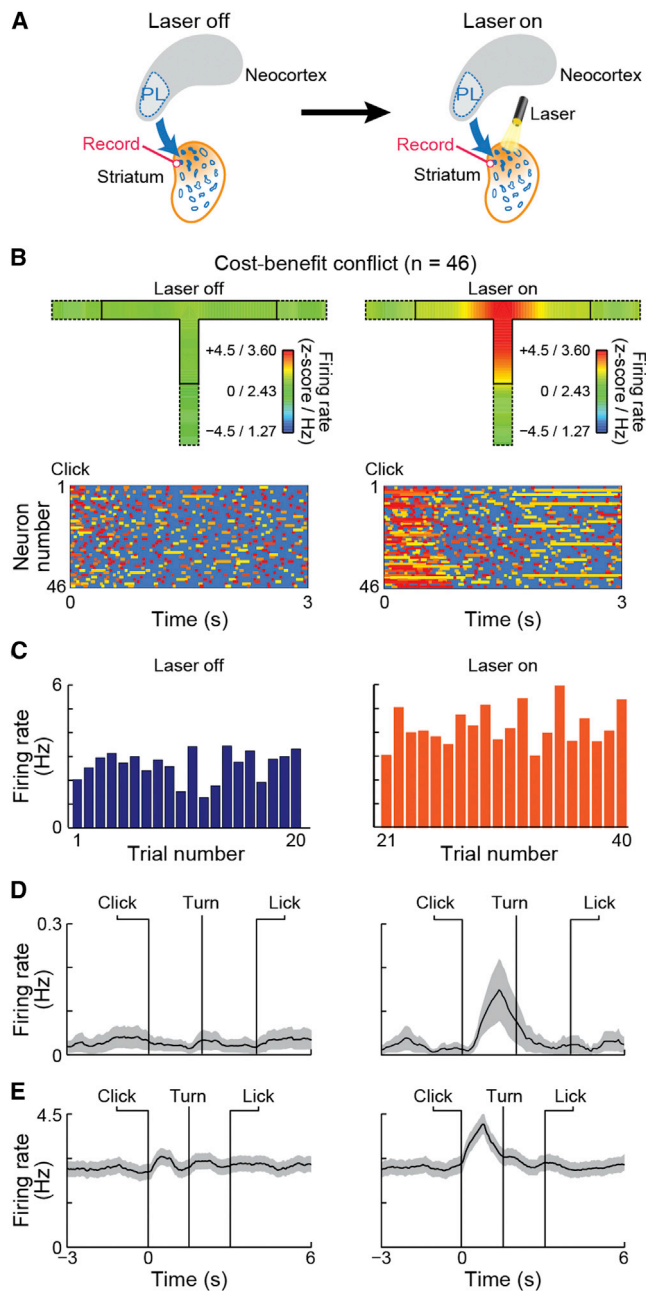
Figure 5. Optogenetic Inhibition of PFC-PL Terminals in Cost-Benefit Conflict Task Increases Firing Rates of Putative Striosomal Neurons

(A) Consecutive cost-benefit conflict task blocks (20 trials each), without, then with, laser inhibition for 3 s, starting at click.

(B) Maze activity plots (above) and burst activity heat maps (below) for 46 putative striosomal SPNs.

(C) Trial-by-trial firing rates across the blocks. p < 0.001, paired t test between blocks.

(D and E) Firing rates (mean ± SEM) for 1 (D) and for 46 (E) putative striosomal SPNs recorded across blocks. p < 0.001, paired t test between blocks. See also Figure S5.

but to a decrease in firing of the HFNs (Figures 6H and S6I). Thus, the uniquely low firing rates of the striosomal SPNs during conflict cost-benefit decision-making likely resulted, at least in part, from task-selective excitation of HFN bursting by PFC-PLs neurons and subsequent diminution of striosomal SPN firing (Supplemental Experimental Procedures).

Computational Modeling Suggests that Optogenetic Inhibition of PFC-PLs Pathway Reduces Sensitivity to Cost

We attempted to infer computationally the internal motivations accompanying decision-making in these tasks (Figures 7A–7F; Supplemental Experimental Procedures). The logistic modeling estimated that the effect of optogenetically inhibiting the PFC-PL pathway targeting striosomes was to halve the sensitivity to cost, and the effect of optogenetically exciting the same pathway was to double the sensitivity to cost, specifically in the cost-benefit conflict task (Figure 7A) but not in the other conditions (Figures 7B and 7C). One interpretation of these findings is that the PFC-PL pathway preferentially targeting striosomes is critical to weighing good and bad options, specifically when the two opponent motivations, here the motivation to approach reward and the motivation to avoid aversive stimulus, are active (Figure 7G).

DISCUSSION

Our findings suggest a remarkable specialization of decision-related corticostriatal circuits, whereby a subset of projection neurons in a single neocortical region can become engaged or disengaged according to the particular subtype of value-based decision to be made. We found that this specialized dynamic allocation of cortical function could be implemented by means of equally context-sensitive striatal microcircuitry engaged by the cortical input (Figure 7H). Strikingly, for the prefronto-striatal circuits that we studied here, these patterns of selective behavioral control were matched to the striosome-matrix architecture of the striatum. Thus the development of differentiated value-based decision-making behavior has a biological expression in the compartmental organization of corticostriatal circuits.

Circuit Analysis of Corticostriatal Function

Our goal in these experiments was to determine circuit-level function in corticostriatal systems, using electrophysiological recording and optogenetic approaches during active implementation of decision-making as animals performed tasks under different value-related contexts and, insofar as feasible, to identify the task-related activity of specific neocortical and striatal cell types through orthodromic and antidromic analyses. We met technical limitations of many sorts, including the fact that the two corticostriatal circuits of our focus preferentially, not exclusively, targeted either striosome or matrix compartment, that our antidromically and orthodromically identified subpopulations were small compared to the total population of neurons recorded, and that we could not specify beyond a regional analysis and by control recording assessments the reach of the optogenetically applied light. Further, although many of our findings relate to the firing activity of neurons during the maze
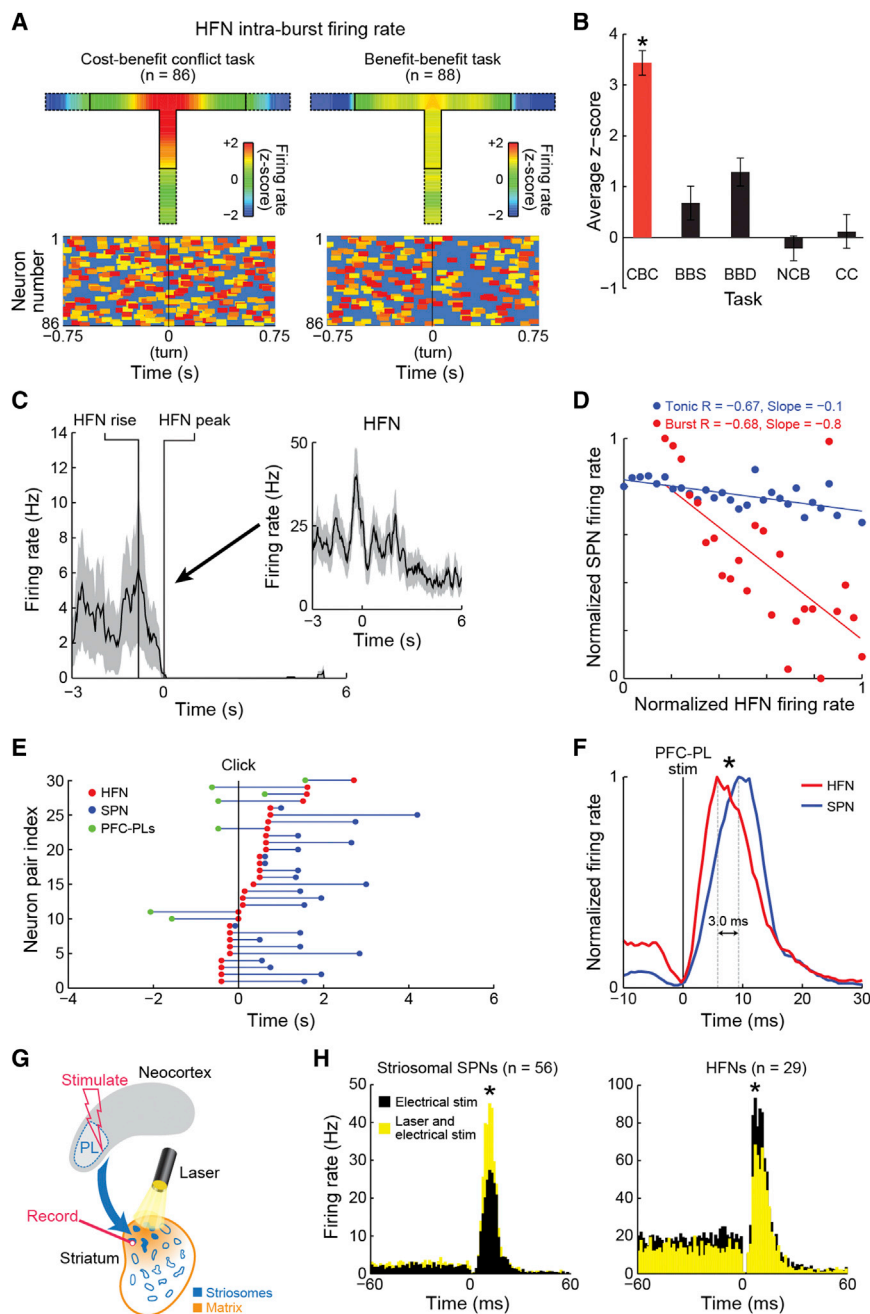
Cell

Figure 6. Sequence of Activity during Cost-Benefit Decision-Making Recorded from PFC-PLs Neurons, Striatal HFNs, and SPNs

(A) Average intra-burst activity (top) and heat maps (bottom) of HFNs during cost-benefit conflict (left) and benefit-benefit (right) tasks.

(B) HFN intra-burst firing rates (mean ± SEM) during click-to-turn periods. *p < 0.001 (two-tailed t test; difference between CBC and other tasks).

(C) Activity of single SPN (mean ± SEM), aligned at zero to activity peak of an HFN (inset) recorded simultaneously by single tetrode. Inset zero indicates time of start click.

(D) Firing rates of a simultaneously recorded HFN-SPN pair, for phasic (burst, red) and tonic (non-burst, blue) HFN activity, with correlation coefficient (R) and slope for each. Dots show SPN activity averaged across all 240 ms bins sorted for HFN firing rates in 5-Hz steps.

(E) Sequence of peak excitation of PFC-PLs neurons (green) and HFNs (red) and peak inhibition of SPNs (blue) recorded in pairs as shown. Plots aligned to start click (zero).

(F) HFN (n = 29, red) and simultaneously recorded SPN (n = 56, blue) responses to PFC-PL stimulation. HFNs lead SPNs by ∼3 ms. *p = 0.001 (Wilcoxon and two-sample Kolmogorov-Smirnov tests).

(G) Stimulation-inhibition protocol with SPN recordings in consecutive blocks of PFC-PL electrical stimulation then combined PFC-PL electrical stimulation and intrastriatal optogenetic inhibition of PFC-PL input.

(H) Putative striosomal SPN and HFN population firing rates aligned to PFC-PL stimulation during the stimulation-only block (black) and stimulation-laser block (yellow). Laser illumination increased SPN firing by 34% but decreased HFN firing by 32%. *p < 0.001 (two-tailed t test).

See also Figure S6.

that we obtained across animals, across behavioral, electrophysiological, and optogenetic findings, and across stimulation-recording experiments.

Motivational Conflict Activates the PFC-PL Pathway Preferentially Targeting Striosomes

Our findings demonstrate a rich repertoire of decision-making capabilities that can be engaged in relation to environmental costs and benefits. Yet, for the five tasks studied here, differing only in their cost and benefit offers, the PFC-PL corticostriatal circuit preferentially targeting striosomes was brought into play during maze runs only in cost-benefit decision-making contexts involving approach-avoidance conflict. Optogenetic inhibition of this pathway had equally selective effects on cost-benefit conflict task performance, increasing approach to high-cost options, yet scarcely changing performance in the other four tasks, including the non-conflict cost-benefit task in which simultaneous evaluation of cost and benefit was still required, but in which the degree
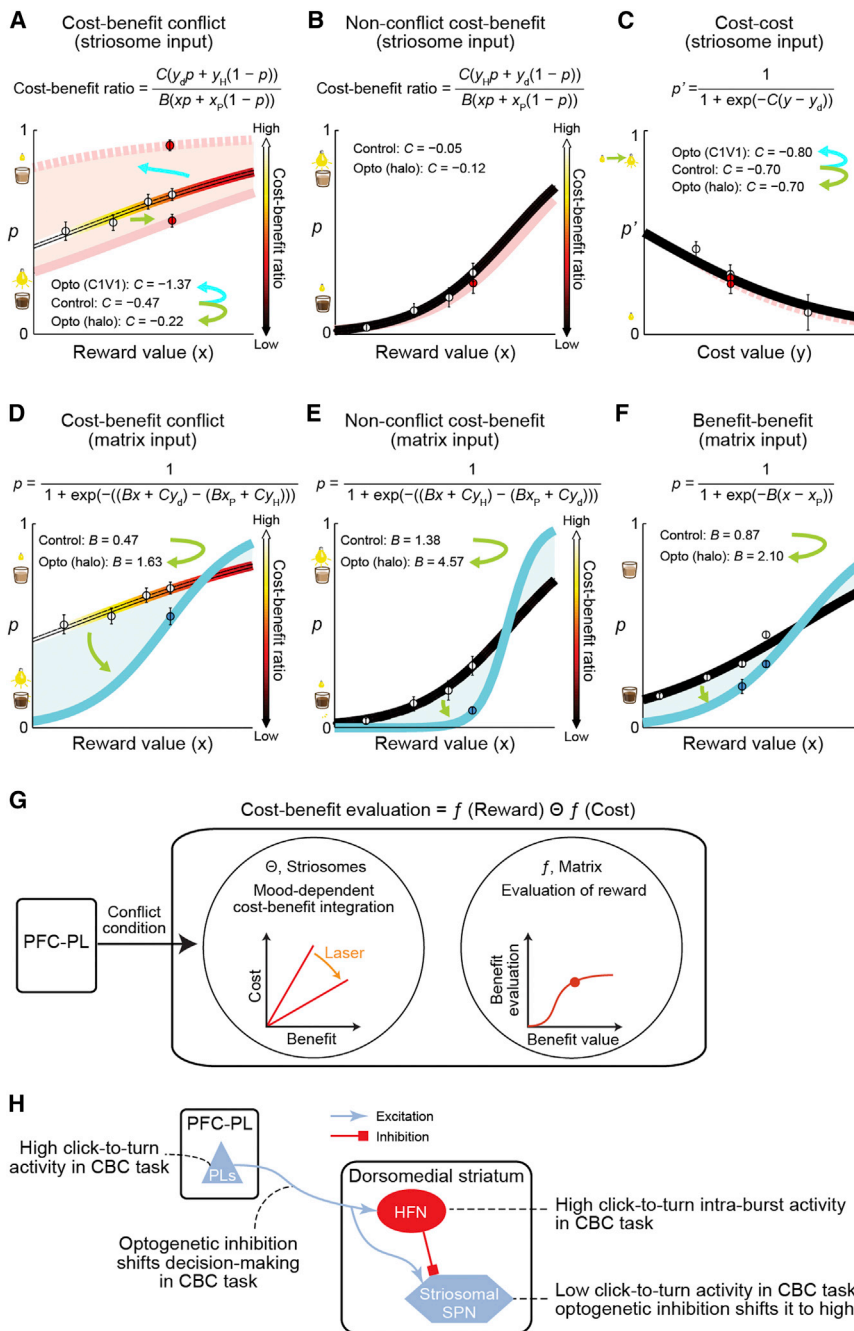
runs, we could not specify the time of decision-making, but rather, had to rely on recording the rats' behavioral responses based on their decisions. Nor did we test decision-making modes with other costs and other benefits, for example, costs based on effort (Rangel and Hare, 2010; Rudebeck et al., 2006; Salamone and Correa, 2012). Further, we used as costs light stimuli, which can produce fear, and although our evidence suggests that fear was not a main driver of the animals' behavior, this issue remains of interest. Despite these and other problems, which we attempt to address in Supplemental Experimental Procedures, we found a striking internal consistency to the results

Figure 7. Computational Models to Characterize the Effects of Optogenetic Manipulations

(A–F) Choice probability (p: probability of choosing diluted chocolate milk; p': probability of choosing bright light) derived from the logistic regression plotted against reward (x) or cost (y) value. For cost-benefit conflict (A and D) and non-conflict cost-benefit (B and E) tasks, lines graded by color indicate cost-benefit ratio (i.e., estimates of motivational conflict). Circles indicate empirically obtained means (filled: optogenetic manipulation, open: control) with SEM. Results of optogenetic manipulations of PFC-PL pathway targeting striosomes (A–C) could be accounted for by change in the sensitivity to cost ("C") under motivational conflict. Solid and dotted pink lines indicate, respectively, the modeled behaviors for optogenetic inhibition (halo) and excitation (C1V1) of the striosome-targeting pathway. Changes in sensitivity to cost were specifically induced in cost-benefit conflict task (A), but not in non-conflict cost-benefit (B) or cost-cost (C) task. Optogenetic inhibition (halo) of PFC-ACC pathway targeting matrix (D–F) could be accounted for by increase in the sensitivity to reward ("B") in the cost-benefit conflict (D), non-conflict cost-benefit (E), and benefit-benefit (F) tasks (blue lines: modeled behaviors for optogenetic inhibition).

(G) Phenomenological model of PFC-PL striosomal circuit function. PFC-PL provides context information about conflict, engages intrastriatal network inhibiting striosomal SPNs in high-conflict context. Matrix evaluates benefits, whereas striosomes integrate cost and benefit when both values are high.

(H) Schematic circuit diagram and summary of major findings.

See also Supplemental Experimental Procedures.

aversion is known to affect strongly choice behavior (Kahneman and Tversky, 1984), suggesting a potential substrate of emotional decision-making.

Such control of approach-avoidance behavior has been intensively studied in experimental animals (Amemori and Graybiel, 2012; Miller, 1971) and also in humans, in whom disturbances of such decision-making have been used as a marker for anxiety disorders (Aupperle et al., 2011; Dickson and MacLeod, 2004). Such a linkage to emotional decision-making and its frailty in some neuropsychiatric disorders accords with much work pointing to the medial prefrontal cortex as having abnormal activity in disorders such as obsessive-compulsive disorder (Fitzgerald et al., 2005), anxiety disorders (Pizzagalli, 2011) including post-traumatic stress disorder (Kasai et al., 2008), and addictive states (Goldstein et al., 2009). The prelimbic region of the rodent prefrontal cortex has also been implicated in behavioral responses to conflict, fear and its control, reward seeking and related functions, as well as

of motivational conflict was negligible. Our computational modeling of these effects singled out sensitivity to cost as a potential variable modified by the optogenetic manipulations.

In the cost-benefit conflict task, a choice of one option satisfies one approach-avoidance motivation (for example, approach) but not the other (for example, avoidance). By choosing the high-cost, high-reward option, the rats had to tolerate bright light, and by choosing the low-cost, low-reward option, the rats had to experience a substantial loss of the potential reward offered on the opposite site. In microeconomics, loss

Cell

in behavioral flexibility, all of which could be related to mood and its control (Sangha et al., 2014; Seamans et al., 1995; Walton et al., 2002).

Here, by comparing behavior and neural activity across performance of multiple tasks, we found that a particular prefronto-striatal circuit can be differentially engaged by conditions inducing approach-avoidance conflict. Thus, the regulation of internal approach-avoidance drives could be an essential part of the functional selectivity of the PFC-PL pathway.

Cost-Benefit Conflict Context Engages Selective Striatal Interneuronal Circuits to Control the Effects of PFC-PL on the Activity of Striosomes

Our physiological experiments demonstrated that PFC-PLs neurons were selectively activated during runs in the cost-benefit conflict task, that striatal HFNs, thought to correspond to inhibitory interneurons, were also selectively activated, but that putative striosomal SPNs were selectively inhibited during these runs. Moreover, in simultaneous recordings from combinations of cortical PFC-PLs neurons and striatal SPNs and HFNs, we observed dynamic sequences in which activity peaks in the PFC-PLs neurons preceded burst activity peaks of the HFNs, which in turn preceded inhibition peaks of the SPNs. Finally, when we electrically stimulated the PFC-PL but optogenetically inhibited its striatal terminals, the inhibition increased the spike firing of putative SPNs but decreased firing of the HFNs.

These results suggest that an inhibitory bursting interneuronal system within the striatum is engaged when the PFC-PLs neurons are activated, and that this intrastriatal system can suppress activity preferentially in striosomes, but only under highly task-dependent conditions. This inversion of excitatory cortical drive into inhibition supports evidence for fast dynamics of high-firing interneurons (Berke, 2011; Burguière et al., 2013; Koós and Tepper, 1999). Our results, however, further suggest that the dynamics of the corticostriatal and intrastriatal circuits are task-selective and are crucial in underpinning the powerful effects of optogenetic manipulation of the PFC-PL pathway to striosomes.

By this account, optogenetic inhibition of the PFC-PL pathway during the high conflict task released activity in the striosomes during the time in which the animals greatly increased their approaches to high-cost, high-benefit goals, and optogenetic excitation of this pathway turned off the striosomes during the time when the animals decreased their approaches to such goals. If this simple interpretation is correct, then striosomal activation would itself be correlated with, and potentially causative to, increased approaches to high-cost options (decreased cost sensitivity), and striosomal shutdown would be related to, and potentially causative to, decreased approach to high-cost options (increased cost sensitivity).

More generally, these findings suggest that the PFC-PL pathway to striosomes is an important controller of behavior elicited by motivational conflict. It is remarkable that these selective effects were not apparent when we applied optogenetic inhibition to PFC-PL terminals in either the ventral tegmental area or the basolateral amygdala, recipients of PFC-PL input, nor even when we applied the inhibition to the PFC-PL itself. All of these findings together, across physiology, behavior and opto-

genetics, point to a specialized function for the circuit preferentially interconnecting the PFC-PL to striosomes.

A Broad Influence of the PFC-ACC Corticostriatal Circuit Preferentially Targeting the Striatal Matrix

With optogenetic inhibition of the PFC-ACC terminals in the same dorsomedial region of the striatum, the rats increased their approaches to higher benefits in all of the tasks. These results suggest that the matrix, at least in the dorsomedial striatum, is involved in evaluating the benefit of the goals and could have less specific relation to cost-benefit integration. Logistic regression analysis suggested that the effect of inhibiting the PFC-ACC terminals in the striatum could be consistently accounted for by an increase in the sensitivity to the benefit component of the goal (increase in approach motivation), regardless of the task condition. Thus within the striatum, the behavioral effects of disconnecting the striosome and matrix compartments from their respective preferential prefrontal inputs were strikingly different.

The Potential Functional Impact of Cortical Control of Striosomes

Striosomes are anatomically in a position to affect the dopamine-containing neurons of the midbrain both directly (Fujiyama et al., 2011; Prensa and Parent, 2001; Watabe-Uchida et al., 2012) and indirectly via the lateral habenula (Rajakumar et al., 1993; Stephenson-Jones et al., 2013), sites that affect mood, motivation, and action (Hong and Hikosaka, 2013; Lak et al., 2014; Stopper et al., 2014). Here, we did not address the potential effects of optogenetic manipulations of the PFC-PL pathway to striosomes on the dopamine-containing neurons of the midbrain. Our findings nevertheless raise the possibility that striosomes could have an impact on decision-making via direct and indirect regulation of dopaminergic signaling.

Our findings demonstrate that a medial prefrontal pathway, here defined in rodents, can profoundly influence the activity of striosomal projection neurons in the dorsomedial part of the striatum. The exquisite selectivity of this control for situations in which motivational conflict was induced by the cost-benefit conflict context suggests that striosomes might influence not only ongoing value-based decision-making but also mood states and state-dependent control of motivation. Striosomes, due to their small size, have not yet be identified in fMRI studies of the human brain and therefore cannot yet be seen in action. They have already been found, however, in clinical studies including post-mortem analysis, to be abnormal in neurologic and neuropsychiatric disorders involving changes in mood and loss of normal motor control (Crittenden and Graybiel, 2011; Tippett et al., 2007). In studies in experimental animals, their activity as judged by gene expression patterns has been associated with insistent, repetitive and stereotyped behaviors (Canales and Graybiel, 2000; Crittenden and Graybiel, 2011).

Our experiments were limited to analysis of cortical inputs to the dorsomedial associative striatum and likely do not expose the full functionality of cortico-striosomal functions. Striosomes exist in regions of the associative striatum that are not at all or only weakly connected with the cortical regions that we manipulated. What we emphasize here is that by manipulating the striatal terminals of the PFC-PL circuit preferentially engaging

Cell

striosomes, we obtained behavioral effects that were context-dependent and that were not matched either by directly manipulating the cortical region itself or by manipulating two other regions targeted by the terminals of this cortical region. The exquisitely specialized corticostriatal striosomal circuit identified here could contribute to these and related disturbances of mood and balanced decision-making under conditions of conflicting motivational demands.

EXPERIMENTAL PROCEDURES

All experimental procedures were approved by the Committee on Animal Care at the Massachusetts Institute of Technology. Adult Long-Evans rats (n = 55) were trained to perform value-based decision-making tasks on a T-maze composed of a running track and two end-arms with light focused on reward feeders. To dissociate reward, cost, and motivational conflict, we used five different types of decision-making tasks: cost-benefit conflict, benefit-benefit with similar reward, benefit-benefit with dissimilar reward, non-conflict cost-benefit and cost-cost (Figures 1A and 1B). We adjusted the cost and reward scales according to the psychometric function of each individual rat. Tasks were presented in random order, but only one cost-benefit conflict session was given per week (Figure S1D). We performed simultaneous cortical and striatal tetrode recordings and optogenetic manipulation to examine functionally corticostriatal circuits anatomically identified as preferentially targeting striosomes (originating in PFC-PL) or matrix (originating in PFC-ACC) in the dorsomedial striatum. For optogenetic experiments, virus encoding halorhodopsin or C1V1, or control virus, was injected into the PFC-PL or PFC-ACC. Light (1.8–2.2 mW) was intrastriatally delivered for 3 s from trial-starting click (Figure 1D). Compartment selectivity of the optogenetic manipulations was estimated by densitometric analysis of EYFP tagged to the opsin (Figure S2). Following each session, electrical microstimulation was delivered to the dorsomedial striatum or PFC-PL to identify, respectively, PFC-PL neurons projecting to the dorsomedial striatum (PFC-PLs neurons) and putative striosomal SPNs (Figure 3). Within the striatum, we identified putative SPNs and HFNs based on their spike waveforms, firing rates and spiking patterns (Figure S3E). Burst activity was extracted by identifying spike trains with short interspike intervals (Figure S6). Z scores of trial activity were calculated using the baseline (11–3 s before the click) firing rate and SD and were plotted onto the maze shape. Behavior and optogenetic effects were modeled using logistic regression. Significant differences were determined by two-tailed t tests (for optogenetic manipulation effects) and by chi-square tests (for spike activity in histograms). More details are given in Supplemental Experimental Procedures.

SUPPLEMENTAL INFORMATION

Supplemental Information includes Supplemental Experimental Procedures and six figures and can be found with this article online at http://dx.doi.org/10.1016/j.cell.2015.04.049.

AUTHOR CONTRIBUTIONS

A.M.G. oversaw the project. A.F., D.H., L.G.G., and A.M.G designed the experiments. A.F., D.H., and S.J.R. performed electrophysiological, optogenetic, and behavioral experiments. A.F., D.H., L.G.G., A.S.H., and A.M.G. analyzed data. D.H., L.G.G., M.H.R., and A.M.G. performed histological imaging and analysis. K.A. performed modeling with input from A.F. and A.M.G. All authors contributed to discussions about the data and their interpretation. A.M.G. wrote the manuscript with input from A.F., D.H., L.G.G., K.A., and M.H.R.

ACKNOWLEDGMENTS

REFERENCES

Amemori, K., and Graybiel, A.M. (2012). Localized microstimulation of primate pregenual cingulate cortex induces negative decision-making. Nat. Neurosci. 15, 776–785.

Aupperle, R.L., and Paulus, M.P. (2010). Neural systems underlying approach and avoidance in anxiety disorders. Dialogues Clin. Neurosci. 12, 517–531.

Aupperle, R.L., Sullivan, S., Melrose, A.J., Paulus, M.P., and Stein, M.B. (2011). A reverse translational approach to quantify approach-avoidance conflict in humans. Behav. Brain Res. 225, 455–463.

Aupperle, R.L., Melrose, A.J., Francisco, A., Paulus, M.P., and Stein, M.B. (2015). Neural substrates of approach-avoidance conflict decision-making. Hum. Brain Mapp. 36, 449–462.

Berke, J.D. (2011). Functional properties of striatal fast-spiking interneurons. Front. Syst. Neurosci. 5, 45.

Burguière, E., Monteiro, P., Feng, G., and Graybiel, A.M. (2013). Optogenetic stimulation of lateral orbitofronto-striatal pathway suppresses compulsive behaviors. Science 340, 1243–1246.

Canales, J.J., and Graybiel, A.M. (2000). A measure of striatal function predicts motor stereotypy. Nat. Neurosci. 3, 377–383.

Crittenden, J.R., and Graybiel, A.M. (2011). Basal ganglia disorders associated with imbalances in the striatal striosome and matrix compartments. Front. Neuroanat. 5, 59.

Dickson, J.M., and MacLeod, A.K. (2004). Approach and avoidance goals and plans: their relationship to anxiety and depression. Cognit. Ther. Res. 28, 415–432.

Donoghue, J.P., and Herkenham, M. (1986). Neostriatal projections from individual cortical fields conform to histochemically distinct striatal compartments in the rat. Brain Res. 365, 397–403.

Dwyer, D.M., Dunn, M.J., Rhodes, S.E., and Killcross, A.S. (2010). Lesions of the prelimbic prefrontal cortex prevent response conflict produced by action-outcome associations. Q. J. Exp. Psychol. (Hove) 63, 417–424.

Eblen, F., and Graybiel, A.M. (1995). Highly restricted origin of prefrontal cortical inputs to striosomes in the macaque monkey. J. Neurosci. 15, 5999–6013.

Etkin, A., Egner, T., Peraza, D.M., Kandel, E.R., and Hirsch, J. (2006). Resolving emotional conflict: a role for the rostral anterior cingulate cortex in modulating activity in the amygdala. Neuron 51, 871–882.

Fitzgerald, K.D., Welsh, R.C., Gehring, W.J., Abelson, J.L., Himle, J.A., Liberzon, I., and Taylor, S.F. (2005). Error-related hyperactivity of the anterior cingulate cortex in obsessive-compulsive disorder. Biol. Psychiatry 57, 287–294.

Flaherty, A.W., and Graybiel, A.M. (1991). Corticostriatal transformations in the primate somatosensory system. Projections from physiologically mapped body-part representations. J. Neurophysiol. 66, 1249–1263.

Flaherty, A.W., and Graybiel, A.M. (1993). Output architecture of the primate putamen. J. Neurosci. 13, 3222–3237.

Fujiyama, F., Sohn, J., Nakano, T., Furuta, T., Nakamura, K.C., Matsuda, W., and Kaneko, T. (2011). Exclusive and common targets of neostriatofugal projections of rat striosome neurons: a single neuron-tracing study using a viral vector. Eur. J. Neurosci. 33, 668–677.

Cell

Gerfen, C.R. (1984). The neostriatal mosaic: compartmentalization of cortico-striatal input and striatonigral output systems. Nature *311*, 461–464.

Gleichgerrcht, E., Ibáñez, A., Roca, M., Torralva, T., and Manes, F. (2010). Decision-making cognition in neurodegenerative diseases. Nat. Rev. Neurol. *6*, 611–623.

Glimcher, P.W., and Fehr, E. (2014). Neuroeconomics: Decision Making and the Brain, Second Edition (New York: Academic Press).

Goldstein, R.Z., Alia-Klein, N., Tomasi, D., Carrillo, J.H., Maloney, T., Woicik, P.A., Wang, R., Telang, F., and Volkow, N.D. (2009). Anterior cingulate cortex hypoactivations to an emotionally salient task in cocaine addiction. Proc. Natl. Acad. Sci. USA *106*, 9453–9458.

Graybiel, A.M. (1990). Neurotransmitters and neuromodulators in the basal ganglia. Trends Neurosci. *13*, 244–254.

Graybiel, A.M., and Ragsdale, C.W., Jr. (1978). Histochemically distinct compartments in the striatum of human, monkeys, and cat demonstrated by ace-tylthiocholinesterase staining. Proc. Natl. Acad. Sci. USA *75*, 5723–5726.

Hong, S., and Hikosaka, O. (2013). Diverse sources of reward value signals in the basal ganglia nuclei transmitted to the lateral habenula in the monkey. Front. Hum. Neurosci. *7*, 778.

Kahneman, D., and Tversky, A. (1984). Choices, values, and frames. Am. Psychol. *39*, 341–350.

Kasai, K., Yamasue, H., Gilbertson, M.W., Shenton, M.E., Rauch, S.L., and Pitman, R.K. (2008). Evidence for acquired pregenual anterior cingulate gray matter loss from a twin study of combat-related posttraumatic stress disorder. Biol. Psychiatry *63*, 550–556.

Kita, H., and Kitai, S.T. (1988). Glutamate decarboxylase immunoreactive neurons in rat neostriatum: their morphological types and populations. Brain Res. *447*, 346–352.

Koós, T., and Tepper, J.M. (1999). Inhibitory control of neostriatal projection neurons by GABAergic interneurons. Nat. Neurosci. *2*, 467–472.

Lak, A., Stauffer, W.R., and Schultz, W. (2014). Dopamine prediction error responses integrate subjective value from different reward dimensions. Proc. Natl. Acad. Sci. USA *111*, 2343–2348.

Milad, M.R., Quirk, G.J., Pitman, R.K., Orr, S.P., Fischl, B., and Rauch, S.L. (2007). A role for the human dorsal anterior cingulate cortex in fear expression. Biol. Psychiatry *62*, 1191–1194.

Miller, N.E. (1971). Selected Papers on Conflict, Displacement, Learned Drives and Theory (Chicago, Illinois: Aldine Atherton).

Newman, H., Liu, F.C., and Graybiel, A.M. (2015). Dynamic ordering of early generated striatal cells destined to form the striosomal compartment of the striatum. J. Comp. Neurol. *523*, 943–962.

Parthasarathy, H.B., Schall, J.D., and Graybiel, A.M. (1992). Distributed but convergent ordering of corticostriatal projections: analysis of the frontal eye field and the supplementary eye field in the macaque monkey. J. Neurosci. *12*, 4468–4488.

Pizzagalli, D.A. (2011). Frontocingulate dysfunction in depression: toward biomarkers of treatment response. Neuropsychopharmacology *36*, 183–206.

Prensa, L., and Parent, A. (2001). The nigrostriatal pathway in the rat: a single-axon study of the relationship between dorsal and ventral tier nigral neurons and the striosome/matrix striatal compartments. J. Neurosci. *21*, 7247–7260.

Rajakumar, N., Elisevich, K., and Flumerfelt, B.A. (1993). Compartmental origin of the striato-entopeduncular projection in the rat. J. Comp. Neurol. *331*, 286–296.

Rangel, A., and Hare, T. (2010). Neural computations associated with goal-directed choice. Curr. Opin. Neurobiol. *20*, 262–270.

Rudebeck, P.H., Walton, M.E., Smyth, A.N., Bannerman, D.M., and Rushworth, M.F. (2006). Separate neural pathways process different decision costs. Nat. Neurosci. *9*, 1161–1168.

Rushworth, M.F., Noonan, M.P., Boorman, E.D., Walton, M.E., and Behrens, T.E. (2011). Frontal cortex and reward-guided learning and decision-making. Neuron *70*, 1054–1069.

Salamone, J.D. (1994). The involvement of nucleus accumbens dopamine in appetitive and aversive motivation. Behav. Brain Res. *61*, 117–133.

Salamone, J.D., and Correa, M. (2012). The mysterious motivational functions of mesolimbic dopamine. Neuron *76*, 470–485.

Sangha, S., Robinson, P.D., Greba, Q., Davies, D.A., and Howland, J.G. (2014). Alterations in reward, fear and safety cue discrimination after inactivation of the rat prelimbic and infralimbic cortices. Neuropsychopharmacology *39*, 2405–2413.

Seamans, J.K., Floresco, S.B., and Phillips, A.G. (1995). Functional differences between the prelimbic and anterior cingulate regions of the rat prefrontal cortex. Behav. Neurosci. *109*, 1063–1073.

St Onge, J.R., and Floresco, S.B. (2010). Prefrontal cortical contribution to risk-based decision making. Cereb. Cortex *20*, 1816–1828.

Stephenson-Jones, M., Kardamakis, A.A., Robertson, B., and Grillner, S. (2013). Independent circuits in the basal ganglia for the evaluation and selection of actions. Proc. Natl. Acad. Sci. USA *110*, E3670–E3679.

Stopper, C.M., Tse, M.T., Montes, D.R., Wiedman, C.R., and Floresco, S.B. (2014). Overriding phasic dopamine signals redirects action selection during risk/reward decision making. Neuron *84*, 177–189.

Tippett, L.J., Waldvogel, H.J., Thomas, S.J., Hogg, V.M., van Roon-Mom, W., Synek, B.J., Graybiel, A.M., and Faull, R.L. (2007). Striosomes and mood dysfunction in Huntington's disease. Brain *130*, 206–221.

Vogel, J.R., Beer, B., and Clody, D.E. (1971). A simple and reliable conflict procedure for testing anti-anxiety agents. Psychopharmacology (Berl.) *21*, 1–7.

Walton, M.E., Bannerman, D.M., and Rushworth, M.F. (2002). The role of rat medial frontal cortex in effort-based decision making. J. Neurosci. *22*, 10996–11003.

Watabe-Uchida, M., Zhu, L., Ogawa, S.K., Vamanrao, A., and Uchida, N. (2012). Whole-brain mapping of direct inputs to midbrain dopamine neurons. Neuron *74*, 858–873.
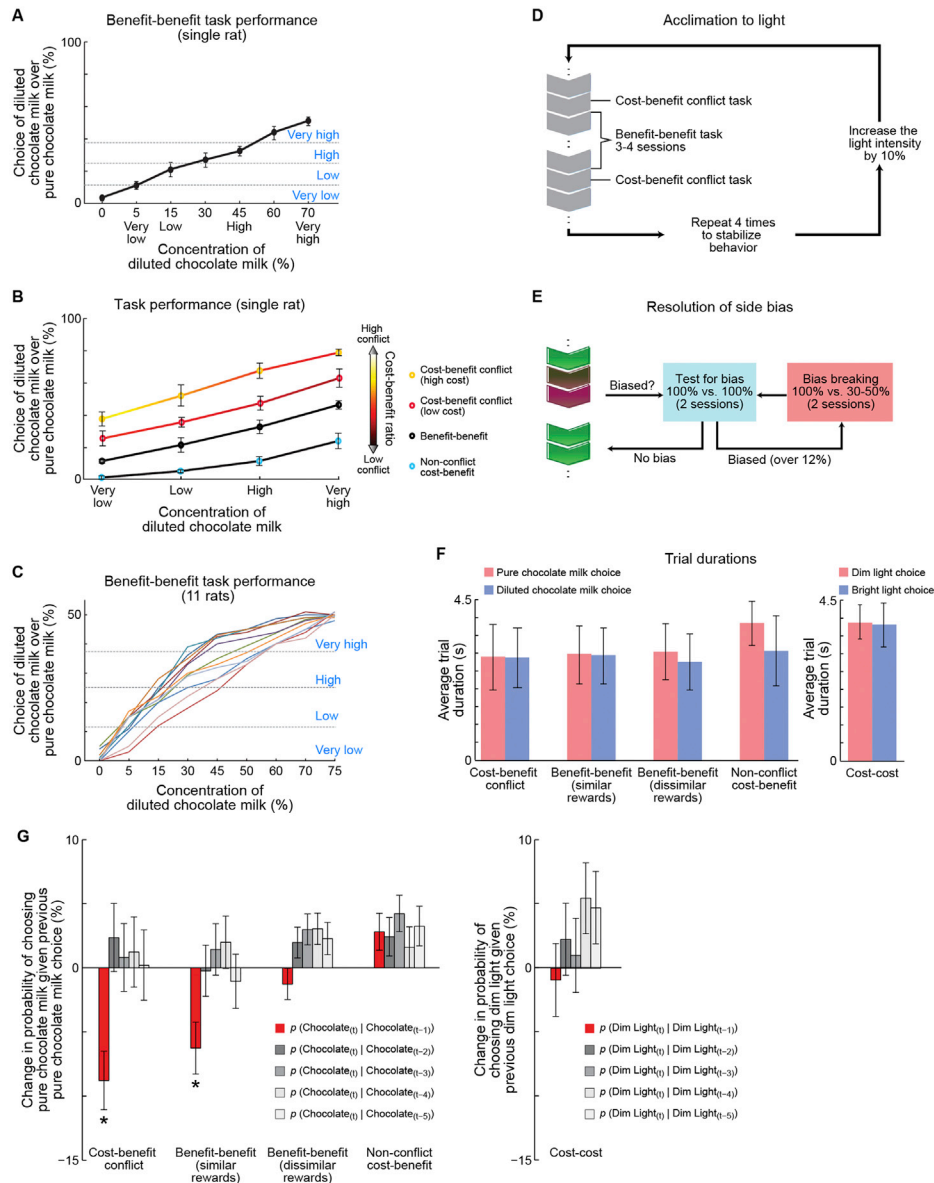
Figure S1. Behavioral Tasks, Related to Figure 1

(A) An example of the change in choice behavior (mean ±SEM) in relation to chocolate milk concentration, obtained from a single rat.

(B) The shift of choice function (mean ±SEM) across variable levels of motivational conflict, observed in a single rat performing cost-benefit conflict, benefit-benefit and non-conflict cost-benefit tasks. Error bars indicate SEM.

(C) Performance of benefit-benefit task by 11 individual rats, each with different psychometric functions, but all exhibiting clear dependence of their choice behavior on the concentration of chocolate milk.

(D) Acclimation to aversive light. Cost-benefit conflict task sessions were separated by at least three sessions of benefit-benefit task. Light intensity was increased over successive sessions.

(E) Measurement and reduction of side bias. Side bias to enter either the left or the right end-arm was reduced through two sessions of a bias-breaking training.

(F) Average running times (mean ±SEM) from click to the first lick were comparable across the different tasks and choices.

(G) Current choice is influenced by previous choice. For each task type, conditional probability of choosing pure chocolate milk (or, in the cost-cost task, dim light) in current trial (t) given choice of pure chocolate milk in previous trial (t−1), two trials before (t−2), three trials before (t−3), four trials before (t−4), or five trials before (t−5) was calculated. Change in probability was calculated by subtracting the unconditional probability of choosing pure chocolate milk (or dim light) and expressing as a percentage. Error bars indicate SEM. *$p < 0.001$ (2-tailed z-test comparing the conditional probability given choice in previous trial (t−1) with that given choice in two to five trials before (i.e., t−2, t−3, t−4 and t−5)).
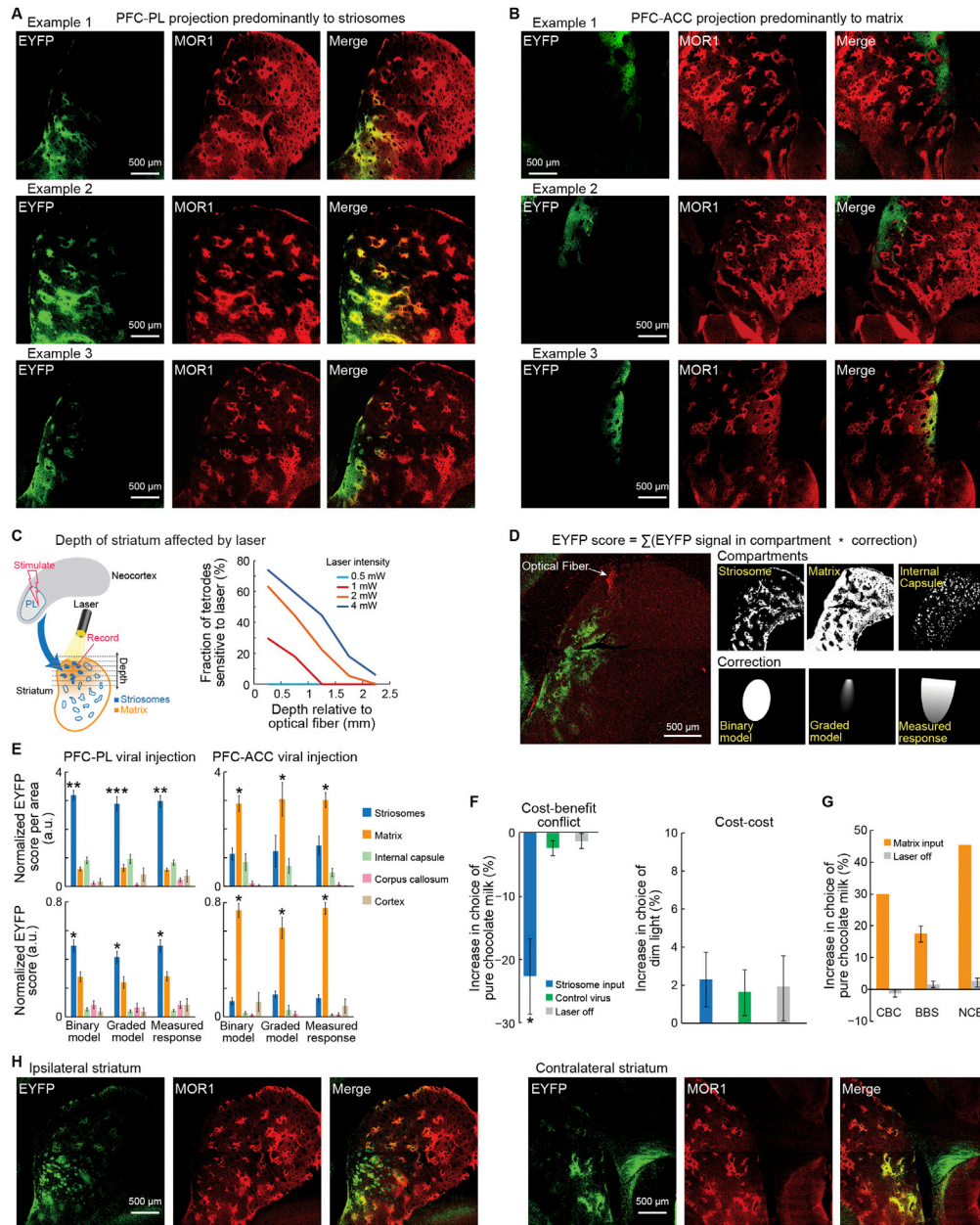
Figure S2. Selectivity of PFC-PL Terminals in Striosomes and PFC-ACC Terminals in Matrix, Related to Figure 2

(A and B) Examples of PFC-PL terminals (A) and PFC-ACC terminals (B) labeled with eNpHR3.0-EYFP in the dorsomedial striatum.

(C) An estimation of depth in the striatum affected by optogenetic manipulation. A comparison is made across two blocks: one with PFC-PL electrical stimulation, and a second with PFC-PL electrical stimulation combined with intrastriatal optogenetic inhibition (left). The percentage of tetrodes responsive to optogenetic inhibition decreased as a function of distance from the optical fiber (right).

(D) A schematic illustration of densitometric analysis. EYFP (green) and CD11 (red) signal in dorsomedial striatum around the tip of the optical fibers was scanned by confocal microscopy (left). The striosome, matrix and other regions identified (e.g., internal capsule, corpus callosum and cortex) were outlined (upper right). Three models were applied for evaluation of the optogenetic effect on each compartment and other regions (lower right). See Densitometric Analysis.

(E) EYFP score per area (upper panels) and EYFP score (bottom panels) for each compartment and region in PFC-PL cases (left panels) and in PFC-ACC cases (right panels). Data are shown as mean ± SEM. *p < 0.05, **p < 0.01, ***p < 0.001 (two-tailed t test).

(F) Behavioral effects (mean ± SEM) of optogenetic stimulation of PFC-PL terminals in cost-benefit conflict (left) and cost-cost (right) tasks. *p < 0.001.

(G) Behavioral effects of optogenetic inhibition of contralateral matrix-predominant inputs (compare with Figure 2D).

(H) Internal capsule fiber bundle labeled with EYFP in ipsilateral (left), but not contralateral (right), dorsomedial striatum.
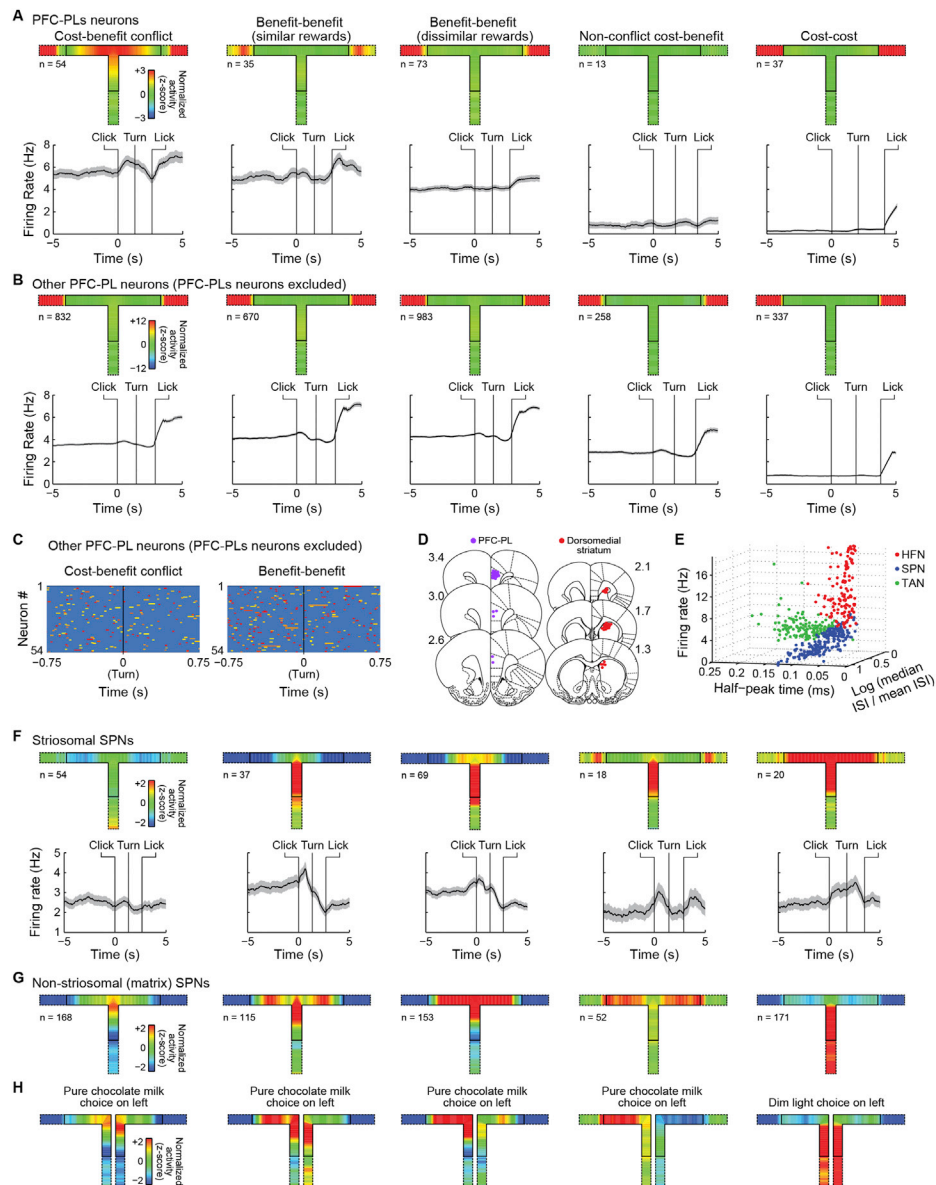
Figure S3. PFC-PL and Striatal Activity during Decision-Making Tasks, Related to Figure 3

(A) PFC-PLs neurons in five decision-making tasks. Activity is represented by mean z-scores in color scale (top) and by firing rates (mean ± SEM) in a ± 5 s period around the click (bottom). Smaller T within the T-maze indicates the period between click and the first lick, and extensions represent 3 s before and after this period.

(B) Activity of the PFC-PL neuronal population excluding the antidromically identified PFC-PLs neurons in five decision-making tasks, plotted as in A. These neurons increased their firing at goal-reaching in every task.

(C) Neuronal burst activity heat map of 54 randomly selected PFC-PL (non PFC-PLs) neurons in cost-benefit conflict task (left) and benefit-benefit task with similar reward (right).

(D) Histologically identified location of tetrodes in the PFC-PL (left) and the dorsomedial striatum (right). Each dot represents the location of a marker lesion. Numbers indicate AP coordinates (mm).

(E) Classification of striatal neurons. HFNs, SPNs and tonically active neurons (TANs, not reported here) are putatively classified through Gaussian mixtures clustering on three dimensions, which combine waveform analysis (x axis), firing rate analysis (y axis) and inter-spike interval (ISI) distribution analysis (z axis).

(F) Striosomal SPNs in five decision-making tasks. Activity is represented by mean z-scores (top) and firing rates (bottom).

(G) Non-striosomal (matrix) SPNs in five decision-making tasks. The non-striosomal SPNs were active in all tasks.

(H) Non-striosomal (matrix) SPN activity averaged for each choice type. Pure chocolate milk (dim light in the cost-cost task) choice presented in left arm of the T-maze. Diluted chocolate milk (bright light in the cost-cost task) choice on the right arm.
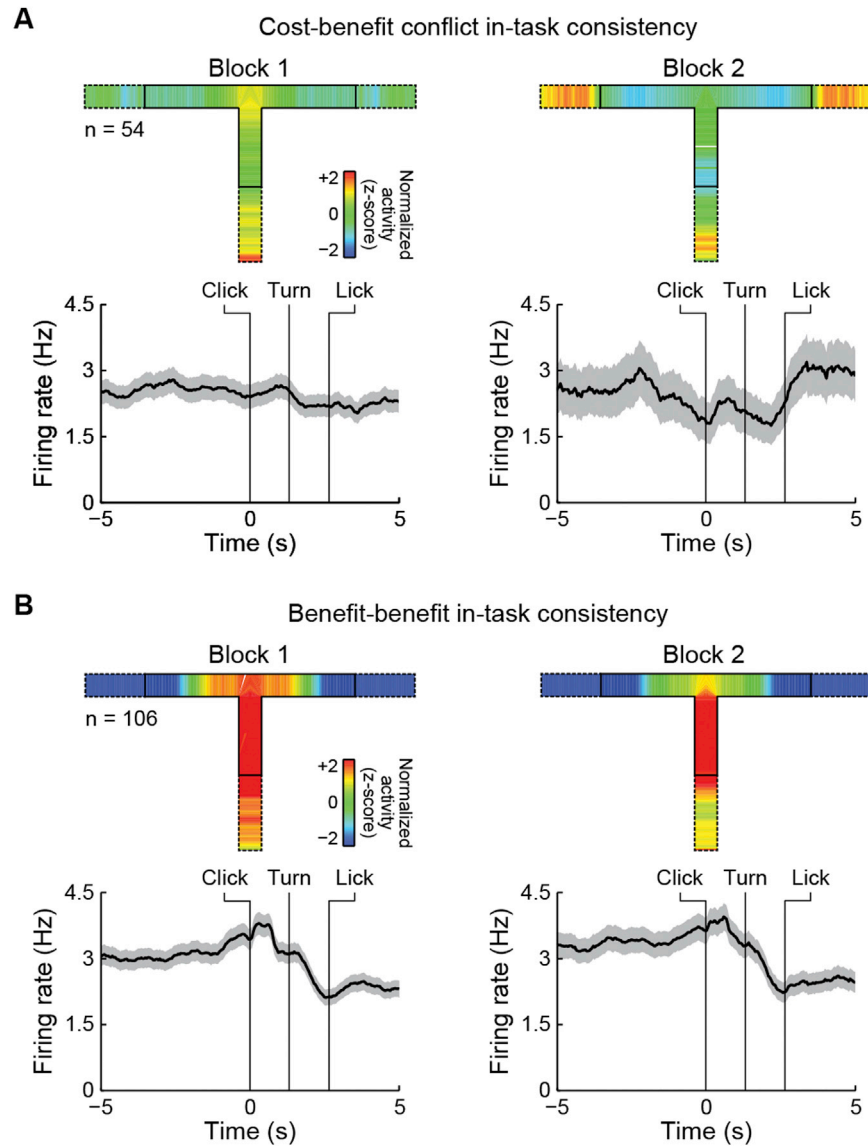
A

Cost-benefit conflict in-task consistency

B

Benefit-benefit in-task consistency

Figure S4. In-Task Consistency of Benefit-Benefit and Cost-Benefit Conflict Tasks, Related to Figure 4

Normalized activity (top) and population firing rate (mean ± SEM, bottom) of putative striosomal SPNs calculated for the first (left) and second (right) 20-trial blocks of a single 40-trial session with cost-benefit conflict task (A) and with benefit-benefit task (B). Activity patterns for the two blocks were statistically identical.
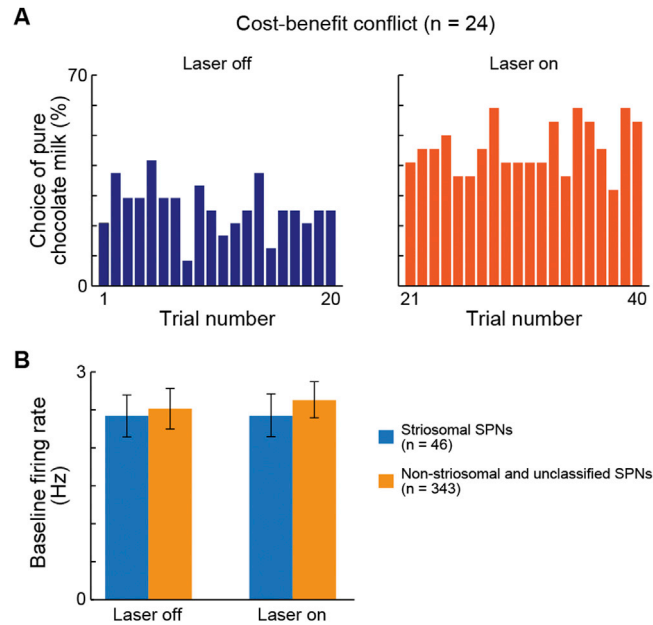
Figure S5. Optogenetic Inhibition of PFC-PL Terminals during Cost-Benefit Conflict Task Has Immediate Effects on Behavior but Not on Striatal Baseline Activity, Related to Figure 5

(A) Trial-by-trial analysis of choices in cost-benefit conflict task averaged over sessions and animals. Percent choice of pure chocolate milk was calculated for each trial of laser-off and laser-on blocks (24 sessions, 5 rats, intrastriatal optogenetic inhibition of striosome-predominant PFC-PL inputs, p < 0.001, chi-square test, between two blocks of the sessions).

(B) Baseline firing rates are unchanged by the optogenetic inhibition. Baseline firing rates (period from 11 to 3 s before click) were computed for striosomal SPNs (blue; n = 46) and all SPNs recorded in the dorsomedial striatum that were not identified as striosomal (orange; n = 343) in laser-on and laser-off blocks. Error bars indicate SEM.
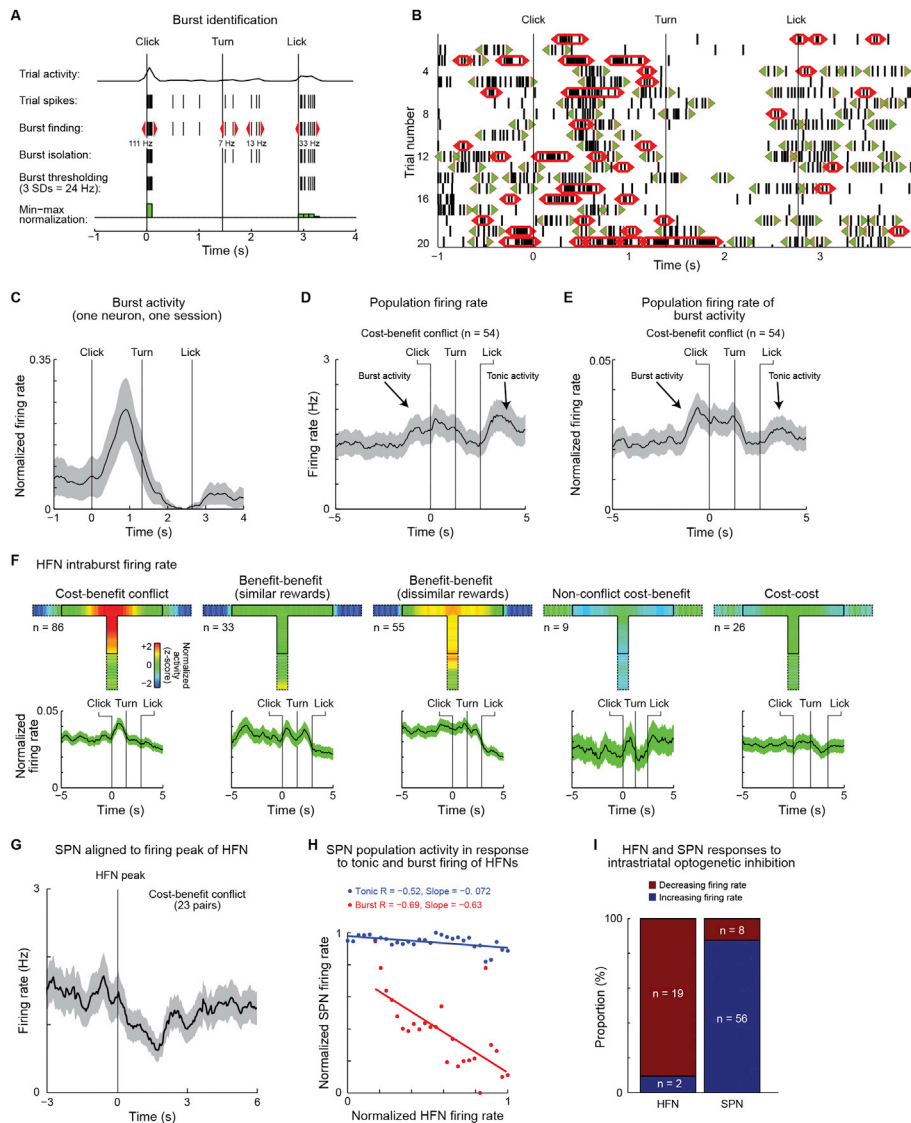
Figure S6. Activity Pattern of HFNs during Decision-Making Tasks, Related to Figure 6

(A) An example of burst extraction, shown for data from one trial. The detection of bursts was a three-step process. First, the start and end points of bursts were identified (red triangles). Second, all non-burst activity was removed (burst isolation), and remaining intra-burst frequency was measured. Third, bursts with frequency higher than 3 SDs above the baseline were kept for analysis (burst thresholding), and firing rates were normalized on a minimum (0) to maximum (1) scale (min-max normalization).

(B) An example of burst detection for one session. The groups of spikes with red outlines were identified as significant bursts (> 3 SDs), while spikes with olive green outlines (< 3 SDs) were identified as non-significant bursts and therefore not included in further analysis.

(C) Example of intra-burst firing rate, min-max normalized and averaged across the session. Shading indicates SEM.

(D) The population firing rate of PFC-PLs neurons in the cost-benefit conflict task includes both burst activity and tonic activity.

(E) Compared to the population firing rate shown in D, the burst analysis on population firing rate has amplified burst activity and reduced tonic activity.

(F) Activity of HFNs in five decision-making tasks, represented by mean z-scores of intra-burst firing rate (top) and min-max normalized intra-burst firing rate (mean ± SEM, bottom).

(G) SPN-HFN pairs were simultaneously recorded by the same tetrode during the cost-benefit conflict task. SPN population activity was aligned to the peak of HFN activity in the pair.

(H) Normalized (min-max) population activity of SPNs relative to HFN burst and tonic activity with firing rates sorted for 5-Hz windows. See Comparison of SPN Activity in Response to Varying Frequency of Phasic (Burst) and Tonic (Non-Burst) HFN Activity.

(I) Proportions of HFNs and SPNs that responded to intrastriatal optogentic inhibition applied concurrently with electrical stimulation of the PFC-PL. First, neurons that have significant response to electrical stimulation of the PFC-PL were identified. Second, instrastriatal inhibition was applied in the striatum along with the PFC-PL stimulation, and the number of HFNs and SPNs that displayed a significant increase or decrease in firing rates was counted.